Computational Mechanics 31 (2003) 3–26 © Springer-Verlag 2003
DOI 10.1007/s00466-002-0389-9

Energy-dissipative momentum-conserving time-stepping algorithms for the dynamics of nonlinear Cosserat rods†

F. Armero, I. Romero

Abstract This paper presents the development of energy-dissipative momentum-conserving algorithms for the numerical integration of the dynamics of nonlinear Cosserat rods. The proposed numerical schemes exhibit a non-negative energy dissipation, controllable through the appropriate algorithmic parameters including an energy-conserving scheme as a particular case. These conservation/dissipation properties are proven rigorously in the general nonlinear setting, accounting specifically for the finite element implementation of the rotational degrees of freedom associated to the motion of the rod's cross-sections. In particular, we consider a direct parameterization of the director fields defining these sections, hence leading to frame-indifferent approximations of the strain measures defining the rod's mechanical response. The robustness added by these considerations when comparing the proposed numerical schemes with existing conserving schemes is illustrated with several representative numerical simulations.

Keywords Cosserat rods, Nonlinear dynamics, High-frequency dissipative time-stepping algorithms, Finite elements

F. Armero (✉), I. Romero[1]
Structural Engineering, Mechanics and Materials,
Department of Civil and Environmental Engineering,
University of California, Berkeley CA 94720, USA
e-mail: armero@ce.berkeley.edu

[1]*Currently at*: E.T.S.I.C.C.P.,
Universidad Politécnica de Madrid, Spain

Dedicated to the memory of Prof. mike Crisfield, for his cheerfulness and cooperation as a colleague and friend over many years.

† Our motivation behind the developments presented in this paper started from a number of very instructive conversations with Professor M.A. Crisfield. His insight in the numerical treatment of the structural problems considered here was unique. It was for us a great privilege to interact with him and enjoy of his friendship. These interactions were always very rewarding, given especially how contagious his enthusiasm for his work was. We would like to dedicate this modest contribution to his memory.

Financial support for this research was provided by the AFOSR under contract no. F49620-00-1-0360 with UC Berkeley. This support is gratefully acknowledged.

1 Introduction

The numerical integration of the dynamics of nonlinear rods has received a great deal of attention recently. Newly formulated theories of Cosserat-type rods, originally presented in Cosserat and Cosserat (1909), appeared in the works of Reissner (1972) and Simo et al. (1985), among others. We refer to the monograph by Antman (1992) and references therein for a relatively recent and complete account. These theories model the motion of a rod in the general three-dimensional space without any restriction on the amount of the deformation, leading to finite deformation theories usually referred to as geometrically exact. The need to consider finite rotations, and hence to work in the general finite group of rotations, adds a significant complexity in these formulations, especially in the development of numerical integration algorithms for the simulation of these structural systems. In this way, we can refer to Cardona and Geradin (1989); Simo and Vu-Quoc (1988) and Ibrahimbegovic (1995), among many others, for references addressing several issues related to these numerical implementations. The book by Crisfield (1997) has also a complete account of many of these developments.

In the case involving the full dynamic response, the strong nonlinearity of the system introduces a challenge for classical time-stepping algorithms. We can quote the Newmark family of time-stepping algorithms as the most commonly known and used scheme among many classical schemes in structural dynamics. We refer to Hughes (1987) for a complete account on these and related methods. After browsing through this and similar references, we can quickly observe that these methods were originally developed in the context of linear problems. Even though their application is usually considered in the nonlinear range, and even works like Kane et al. (2000) have reconsidered their analysis recently, the number of works in the recent literature identifying the limitation of these methods when applied to nonlinear problems is already significant. We refer to Simo and Tarnow (1992) and Armero and Romero (2001a), among others, for an illustration. The basic limitation of classical schemes like Newmark or even the so-called HHT scheme [Hiber et al. (1977)], Wilson-ϑ method [Wilson (1968)] and other so-called (linearly) "dissipative" schemes, is the appearance of numerical instabilities even though the method is unconditionally stable in the linear range. These instabilities are usually associated with an uncontrollable growth of the energy in the discrete system.

Motivated by these limited stability properties, the search for algorithms that conserve the total energy of the system has received an important amount of attention; see e.g Simo and Tarnow (1992); Crisfield and Shi (1994); Simo et al. (1995); Armero and Petocz (1996) and Gonzalez (2000) for just a few references considering different applications in nonlinear solid mechanics, including nonlinear elastic rods, the case of interest here. The fact that the discrete dynamics generated by the numerical algorithm should inherit the conservation laws of linear and angular momenta was identified as a fundamental property to impose on the integration schemes. Furthermore, the conservation of energy allowed also a more stable simulation of these mechanical systems. But it soon became clear that the high numerical stiffness of these systems led to serious difficulties in completing the simulation and put severe limitations even on these newly developed methods. This numerical stiffness can be traced back to the different mechanical stiffness of the different modes of deformation of the solid: axial, transverse shear, bending and torsion for the rods of interest here. The requirement that the numerical scheme should resolve the wide spectrum of responses generated by these different components proves to be a task too demanding for the time-stepping scheme, especially given the fact that the spatial discretization already introduces a great amount of error when approximating the high-frequency response of the system.

This is exactly the same situation that motivated the development of the aforementioned "linearly dissipative" schemes in the linear range. In this way, numerical schemes that introduce a controllable numerical dissipation in the high-frequency response of the system have been clearly favored not only in the literature but in common practice. We can also quote the related concepts of L-stability [see e.g. Hairer and Wanner (1991)] or of "stiffly accurate" methods [Prothero and Robinson (1974)] in the context of Runge–Kutta methods. Unfortunately, these dissipation properties do not extend again to the nonlinear range, a situation that has motivated an extensive literature in the search of new dissipative numerical schemes for nonlinear problems. We refer to the works of Bauchau et al. (1995); Bauchau and Theron (1996); Kuhl and Ramm (1996, 2001); Kuhl and Crisfield (1997); Botasso and Borri (1997); Botasso et al. (2001) and Armero and Romero (2001a, b), among others.

But beyond these general considerations, one should assure that the dissipative schemes exhibit several additional important properties besides the energy dissipation itself. In this way, we consider fundamental to impose the following requirements to the conserving/dissipative schemes for the mechanical problems of interest:

1. A minimum of second-order accuracy in time.
2. The unconditional character of the non-negative energy dissipation in the time step and material model.
3. The controllable character of this numerical energy dissipation through the appropriate algorithmic parameters, obtaining an energy conserving scheme as a particular case.
4. The numerical scheme must introduce dissipation in the high-frequency range, this understood when applied to a linear problem.
5. The scheme must inherit the conservation laws of the exact (physical) linear and angular momenta in the full nonlinear range, and preserve exactly the associated relative equilibria. In fact, and related to this latter property, the scheme must introduce the dissipation in the internal modes of the motion of the system, while leading to a conservative approximation of the group motions associated to the symmetries and conservation laws acting on the system.
6. The scheme must be competitive in terms of computational cost, favoring one-step self-starting schemes with no multi-stages.

We refer to Armero and Romero (2001a, b) for a complete discussion of all these aspects together with the developments of new numerical schemes exhibiting all these properties in the context of nonlinear elastodynamics. We call these methods EDMC schemes in short, an acronym for energy–dissipative, momentum–conserving schemes.

An added difficulty was observed by Crisfield and Jelenić (1998) and Jelenić and Crisfield (1999) for the case of rod formulations: finite element implementations of the type presented in Simo (1985) and Cardona and Geradin (1989), among others, based on a direct interpolation of the rotational parameters (usually the total, the incremental or the iterative rotation vector) are not material frame indifferent. This is a fundamental property of the underlying physical theory by which the strain measures and the associated stress resultants given by the constitutive relations are not affected by superimposed rigid body motions. This shortfall of the aforementioned numerical models was related to the nonlinear relation between the rotation parameters and the finite rotation tensor, and how this relation was affected by the spatial discretization of the former. In some cases, it was also observed that the solutions for hyperelastic problems were even path-dependent. Co–rotational formulations were proposed in Crisfield and Jelenić (1997, 1998); Jelenić and Crisfield (1998, 1999, 2000) and Galvanetto and Crisfield (1996) that avoided these difficulties. Nonetheless, no extensions to the fully dynamic case could be developed to our knowledge in this co–rotational framework that resulted in the exact energy conservation.

We have recently presented in Armero and Romero (2001c) an alternative parameterization of the rod model that allows for this frame indifferent finite element approximation and leads naturally to energy–momentum conserving schemes for the integration of the rod's dynamics. In fact, we have observed in Romero and Armero (2002a) that similar techniques formulated at the level of interpolated rotational parameters do not lead to these conservation properties. The formulation is based on a direct use of the director field defining the position of the cross–sections with respect to the middle axis, as described in the following section, and its finite element interpolation. This alternative parameterization and corresponding finite element interpolation leads naturally to energy–momentum schemes, while assuring a frame

indifferent approximation of the rod's strain and stress measures. We also refer to Gruttman et al. (1998) and Betsch and Steinmann (2002) for similar formulations in the static case, the later considering Lagrange multipliers on the director fields to impose the rotational constraints.

However, and as discussed above, energy conserving algorithms lack the required robustness to deal with the high numerical stiffness of the problems of interest in this type of applications. It is precisely the goal of this paper to develop energy–dissipative momentum–conserving algorithms for the nonlinear dynamics of Cosserat rods that show this improved robustness. Our starting point is the rod's formulation first presented in Armero and Romero (2001c) and fully developed in Romero and Armero (2002a) and the development of this type of schemes presented in Armero and Romero (2001a,b) for the simpler setting of nonlinear continuum elastodynamics and in Romero and Armero (2002b) for the case of nonlinear shells involving a single director field. The presence in the rod model of different directors (in fact, a director frame consisting of three orthonormal vectors and hence requiring the consideration of the full rotation group) makes this extension non-trivial and deserving this separate treatment. The considered methodology reduces the formulation of the new schemes to the design of the proper dissipation functions defined locally at the quadrature points of a typical finite element implementation. Different dissipation functions are identified for the aforementioned different modes of the rod's deformation as well as the different generalized velocities associated to the translational inertia of the rod's middle axis and to the rotational inertia of the rod's cross–section. In particular, specific functions defined in terms of the full tensor of inertia associated to this cross–section frame needs to be determined in comparison, for example, with prior developments for shells or three-dimensional continuum solids. We present here these new developments, including rigorous proofs of the conservation/dissipation properties of the final schemes. Very importantly these proofs consider the fully discrete system of equations, that is, involving the spatial finite element interpolation and the temporal discretizations. A complete evaluation of the final numerical schemes is also presented through a number of representative numerical simulations.

An outline of the rest of the paper is as follows. We present in Sect. 2 a brief summary of the rod formulation considered in this paper, including a short statement of the conservation properties of interest. Section 3 develops the new energy–dissipative momentum–conserving schemes proposed in this work. We start with a brief but crucial description of the finite element interpolations of the configuration and velocity variables and their variations in Sect. 3.1. It is in this context that we develop the time-stepping algorithms in Sects. 3.2 and 3.3, including the analysis of the conservation/dissipation properties of the final schemes. The numerical implementation of these equations is discussed in Sect. 4, with different representative numerical simulations presented in Sect. 5 to illustrate the performance of the new schemes. Finally, we conclude with a brief summary and some concluding remarks in Sect. 6.

2
The rod model

We summarize in this section the governing equations for a two-director Cosserat rod model. The model is based on the Reissner–Simo formulation as described in Simo (1985). The specific form of the equations considered here follows the parametrization elaborated in Romero and Armero (2002a), in which the directors appear explicitly as part of the kinematic variables. This parameterization is crucial for the algorithmic properties of the numerical discretization presented in the following sections. We refer to these references for further details about the rod model summarized in this section.

2.1
The rod's kinematics

Consider the reference placement of a rod defining the curve $\mathcal{C}^o \in \mathbb{R}^3$, referred to generically as the rod's (reference) middle-axis. Let S and L denote the arclength and the total length of the curve $\mathcal{C}^o$, respectively. Similarly, we denote by $\mathcal{C}$ the curve representing the rod's middle-axis in a generic deformed configuration of the rod. We denote by $\mathbf{r}(S)$ the position vectors of the points in the middle-axis $\mathcal{C}$, still parameterized by the arc-length S as they correspond to the points in the reference middle-axis $\mathcal{C}^o$. This reference middle-axis is represented by the position vectors $\mathbf{r}^o(S)$.

The rod theory of interest here is fully determined by the consideration of a plane cross-section $\mathcal{A}$ at each point S of the middle-axis (i.e. $\mathcal{A}(S)$), with these cross-sections remaining plane and undirstorted during the deformation of the rod. In this way, the position of every section is determined by two orthonormal directors $\{\mathbf{d}_1(S), \mathbf{d}_2(S)\}$. Figure 1 illustrates all these considerations. Following the notation introduced above for the middle-axis, we denote

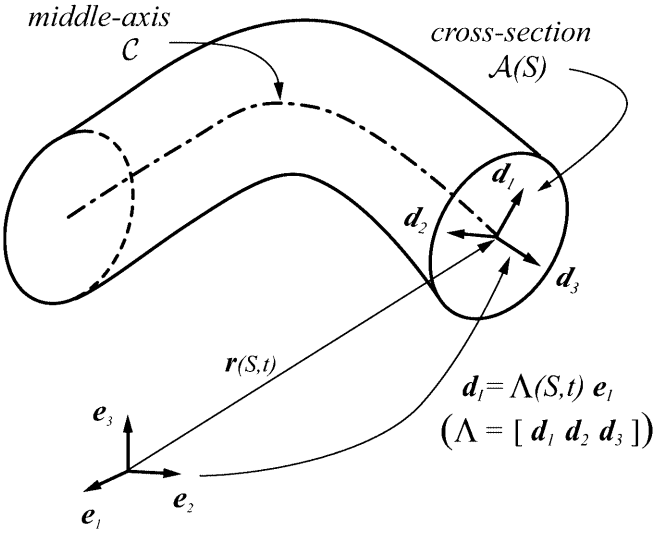

Fig. 1. Definition of a Cosserat rod. The rod motion is determined by following the position vector $\mathbf{r}(S,t)$ of the middle-axis $\mathcal{C}$ and the director frame $\{\mathbf{d}_1, \mathbf{d}_2, \mathbf{d}_3\}(S,t)$ defining the plane cross–section $\mathcal{A}(S)$, all parameterized in terms of the arc-length S of the middle-axis of a reference configuration of the rod. The latter is expressed by the rotation matrix $\mathbf{\Lambda}$ from a fixed Cartesian frame $\{\mathbf{e}_1, \mathbf{e}_2, \mathbf{e}_3\}$

by $\mathbf{d}_\alpha^o$ $\alpha = 1,2$ the directors in the reference placement of the rod. Furthermore, it proves convenient to define the middle-axis as the curve of centroids of the different cross-sections.

The kinematics of the rod is then fully characterized by the configuration space

$$Q = \{\mathbf{\Phi} = (\mathbf{r}, \mathbf{d}_1, \mathbf{d}_2) \in \mathbb{R}^3 \times S^2 \times S^2,\ \ \mathbf{d}_1 \cdot \mathbf{d}_2 = 0,$$
$$\mathbf{\Phi} = \bar{\mathbf{\Phi}} = (\bar{\mathbf{r}}, \bar{\mathbf{d}}_1, \bar{\mathbf{d}}_2) \text{ on } \Gamma_u\} \ , \tag{2.1}$$

where S^2 is the unit sphere in $\mathbb{R}^3$. Here, we have denoted the boundary of the middle-axis $\mathcal{C}$ by Γ and partitioned it as $\Gamma = \overline{\Gamma_t \cup \Gamma_u}$ with $\Gamma_t \cap \Gamma_u = \emptyset$, for Γ_t corresponding to the part of the boundary where external forces are imposed and Γ_u to the rest, where the displacements are known to be the given values $(\bar{\mathbf{r}}, \bar{\mathbf{d}}_1, \bar{\mathbf{d}}_2)$. The latter, the so-called essential boundary conditions, appear explicitly in the definition of the configuration manifold (2.1).

Let "$\times$" denote the vector product in $\mathbb{R}^3$ and define $\mathbf{d}_3(S) = \mathbf{d}_1(S) \times \mathbf{d}_2(S)$, a third director associated with the cross-section at every point S in $\mathcal{C}$. Clearly, the director $\mathbf{d}_3$ is orthogonal to the cross–section. For later use, we introduce the matrix with columns defined by these three directors, that is, $\mathbf{\Lambda}(S) = [\mathbf{d}_1(S)\ \mathbf{d}_2(S)\ \mathbf{d}_3(S)]$. We have then, by construction, that $\mathbf{\Lambda} \in SO(3)$ the group of rotations (i.e. $\mathbf{\Lambda}^{\mathrm{T}}\mathbf{\Lambda} = \mathbf{\Lambda}\mathbf{\Lambda}^{\mathrm{T}} = \mathbf{1}$ with $\det \mathbf{\Lambda} = +1$). The matrix $\mathbf{\Lambda}$ and its counterpart $\mathbf{\Lambda}^o$ in the reference placement of the rod provide a compact notation to refer to the individual directors. In this way, to every configuration $\mathbf{\Phi} = (\mathbf{r}, \mathbf{d}_1, \mathbf{d}_2)$ we associate the equivalent pair $\tilde{\mathbf{\Phi}} = (\mathbf{r}, \mathbf{\Lambda})$, where $\mathbf{\Lambda}$ is the orthogonal matrix with columns $[\mathbf{d}_1\ \mathbf{d}_2\ \mathbf{d}_1 \times \mathbf{d}_2]$, being then the configuration manifold Q isomorphic to $\mathbb{R}^3 \times SO(3)$. The presence of the finite group of rotations in the configuration manifold of the system of interest requires a careful consideration of its variations and rates, as considered in the following section.

2.2
The rod's dynamics

A motion of the rod is a one parameter family of configurations $\mathbf{\Phi}_t$ in Q, where the parameter t is the time. The velocity fields associated to the generalized displacements defining the configuration manifold (2.1) are defined by the material time derivatives

$$\mathbf{v}(S,t) = \dot{\mathbf{r}}(S,t) \quad \text{and} \quad \mathbf{v}_\alpha(S,t) = \dot{\mathbf{d}}_\alpha(S,t), \ \text{for } \alpha = 1,2 \ , \tag{2.2}$$

where the notation $(\dot{\cdot}) = \frac{\partial}{\partial t}(\cdot)\big|_{S \text{ fixed}}$ has been employed. Since the two section directors $\{\mathbf{d}_1, \mathbf{d}_2\}$ must remain orthogonal at all times there exists a unique vector $\boldsymbol{\omega} \in \mathbb{R}^3$ such that

$$\mathbf{v}_\alpha = \boldsymbol{\omega} \times \mathbf{d}_\alpha, \quad \text{for } \alpha = 1,2 \ . \tag{2.3}$$

This vector $\boldsymbol{\omega}$ is the angular velocity of the orthogonal frame composed of the three directors $\{\mathbf{d}_1, \mathbf{d}_2, \mathbf{d}_3\}$. Equation (2.3) can also be expressed in terms of the rotation matrix $\mathbf{\Lambda}$ introduced above as $\dot{\mathbf{\Lambda}} = \hat{\boldsymbol{\omega}}\mathbf{\Lambda}$, where

$$\hat{\boldsymbol{\omega}}\mathbf{a} = \boldsymbol{\omega} \times \mathbf{a} \quad \text{forall } \mathbf{a} \in \mathbb{R}^3 \ , \tag{2.4}$$

associating the axial vector $\boldsymbol{\omega} \in \mathbb{R}^3$ to the skew tensor $\hat{\boldsymbol{\omega}} \in so(3)$ (the linear space of skew tensors). This mapping defines an isomorphism between these two linear spaces. In this way, the set of generalized velocities $\mathbf{W} = (\mathbf{v}, \mathbf{v}_1, \mathbf{v}_2)$ is given by the linear space

$$\mathcal{W} = \{\mathbf{W} = (\mathbf{v}, \mathbf{v}_1, \mathbf{v}_2)_{\mathbf{\Phi}}, \mathbf{v} \in \mathbb{R}^3,\ \mathbf{v}_\alpha = \boldsymbol{\omega} \times \mathbf{d}_\alpha,\ \boldsymbol{\omega} \in \mathbb{R}^3\} \ , \tag{2.5}$$

at each configuration $\mathbf{\Phi} = (\mathbf{r}, \mathbf{d}_1, \mathbf{d}_2)$. We observe that the relations (2.2) defining pointwise the generalized velocities from the configuration variables also apply to the boundary values imposed on Γ_u in the original configuration space (2.1).

The dynamic response of the rod is then characterized by an inertia to the motion of the middle-axis (or translational inertia) and to the motion of the cross-section (or rotational inertia). This defines the total kinetic energy of the rod of the form

$$K(t) := \int_0^L \underbrace{\left(\frac{1}{2} A_{\rho_o}\ \mathbf{v} \cdot \mathbf{v} + \frac{1}{2} \mathcal{I}_{\rho_o}^{\alpha\beta} \mathbf{v}_\alpha \cdot \mathbf{v}_\beta\right)}_{\mathcal{K}_{\rho_o}(\mathbf{v}, \mathbf{v}_1, \mathbf{v}_2)} \mathrm{d}S \ , \tag{2.6}$$

for the kinetic energy density $\mathcal{K}_{\rho_o}$, with the two terms in (2.6) corresponding to aforementioned contributions. In this equation, and in the rest of the paper, the summation convention over repeated indices is adopted, where Greek indices run from 1 to 2 and Latin indices run from 1 to 3. The symbol "$\cdot$" in (2.6) denotes the usual Euclidean inner product in $\mathbb{R}^3$.

The translational inertia is given by the reference mass per unit length $A_{\rho_o}(S)$ and the rotational inertia by the (symmetric, positive definite) Euler dyadic of the cross-section $\mathcal{I}_{\rho_o}(S)$. These quantities are given physically by the relations

$$A_{\rho_o}(S) = \int_{\mathcal{A}(S)} \rho_o \, \mathrm{d}A \quad \text{and} \quad \mathcal{I}_{\rho_o}^{\alpha\beta}(S) = \int_{\mathcal{A}(S)} \rho_o \ \xi^\alpha \xi^\beta \, \mathrm{d}A \ , \tag{2.7}$$

in terms of the reference density $\rho_o = \hat{\rho}_o(\xi^1, \xi^2; S)$ of the material. Here, we have denoted by (ξ^1, ξ^2) the Cartesian coordinates of a point in a given cross–section $\mathcal{A}(S)$ with respect to the planar frame $\{\mathbf{d}_1, \mathbf{d}_2\}$, so $\mathrm{d}A = d\xi^1 d\xi^2$.

2.3
The rod's mechanical response: the strain measures and stress resultants

The mechanical response of the rod is defined through the properly invariant strain and stress tensors measuring the state of deformation of the rod and the internal forces resulting from it. The following strain measures were proposed in Simo (1985)

$$\mathbf{\Gamma}(\mathbf{\Phi}) = \mathbf{\Lambda}^{\mathrm{T}} \mathbf{r}_{,s} - \mathbf{\Lambda}^{o\mathrm{T}} \mathbf{r}_{,s}^o \in \mathbb{R}^3 \quad \text{and}$$
$$\mathbf{\Omega}(\mathbf{\Phi}) = \text{axial}\left[\mathbf{\Lambda}^{\mathrm{T}} \mathbf{\Lambda}_{,s} - \mathbf{\Lambda}^{o\mathrm{T}} \mathbf{\Lambda}_{,s}^o\right] \in \mathbb{R}^3 \ , \tag{2.8}$$

where "axial$[\cdot]$" denotes the axial vector associated to a skew tensor by (2.4) and "$(\cdot)_{,s}$" denotes the partial derivative with respect to the middle-axis coordinate

S. Expanding these definitions in terms of the configuration variables, we have the explicit expressions

$$\boldsymbol{\Gamma} = \left\{ \begin{array}{c} \mathbf{d}_1 \cdot \mathbf{r}_{,s} - \mathbf{d}_1^0 \cdot \mathbf{r}_{,s}^o \\ \mathbf{d}_2 \cdot \mathbf{r}_{,s} - \mathbf{d}_2^o \cdot \mathbf{r}_{,s}^o \\ \mathbf{d}_3 \cdot \mathbf{r}_{,s} - \mathbf{d}_3^o \cdot \mathbf{r}_{,s}^o \end{array} \right\},$$

$$\boldsymbol{\Omega} = \frac{1}{2} \left\{ \begin{array}{c} \mathbf{d}_3 \cdot \mathbf{d}_{2,s} - \mathbf{d}_2 \cdot \mathbf{d}_{3,s} - \mathbf{d}_3^o \cdot \mathbf{d}_{2,s}^o + \mathbf{d}_2^o \cdot \mathbf{d}_{3,s}^o \\ \mathbf{d}_1 \cdot \mathbf{d}_{3,s} - \mathbf{d}_3 \cdot \mathbf{d}_{1,s} - \mathbf{d}_1^o \cdot \mathbf{d}_{3,s}^o + \mathbf{d}_3^o \cdot \mathbf{d}_{1,s}^o \\ \mathbf{d}_2 \cdot \mathbf{d}_{1,s} - \mathbf{d}_1 \cdot \mathbf{d}_{2,s} - \mathbf{d}_2^o \cdot \mathbf{d}_{1,s}^o + \mathbf{d}_2^o \cdot \mathbf{d}_{1,s}^o \end{array} \right\} , \tag{2.9}$$

where we have not made use of the orthogonality of the directors in this last expression given the finite element implementation considered later in this work.

We can observe that both strain measures vanish in the reference configuration and that they are invariant under superposed rigid body motions, namely

$$\boldsymbol{\Gamma}(\boldsymbol{\Phi}^*) = \boldsymbol{\Gamma}(\boldsymbol{\Phi}) \quad \text{and} \quad \boldsymbol{\Omega}(\boldsymbol{\Phi}^*) = \boldsymbol{\Omega}(\boldsymbol{\Phi}) \ , \tag{2.10}$$

with $\boldsymbol{\Phi} = (\mathbf{r}, \mathbf{d}_1, \mathbf{d}_2) \in Q$ and $\boldsymbol{\Phi}^* = (\mathbf{Q}\mathbf{r} + \mathbf{u}, \mathbf{Q}\mathbf{d}_1, \mathbf{Q}\mathbf{d}_2)$ for a vector $\mathbf{u} \in \mathbb{R}^3$ and an orthogonal tensor $\mathbf{Q} \in SO(3)$ defining an arbitrary superimposed rigid body motion. The components of the vector $\boldsymbol{\Gamma}$ can be identified with the transverse shear and axial strains, and those of the vector $\boldsymbol{\Omega}$ with the bending and torsional strains. These strain measures can be obtained from the equations of three dimensional nonlinear elasticity by a projection that accounts for the particular form of the rod's kinematics. Once again, we refer to Simo (1985) for further details on this interpretation.

Conjugate stress measures (or stress resultants) are obtained for an hyperelastic rod, the case of interest here, in terms of an elastic potential $W(\boldsymbol{\Gamma}, \boldsymbol{\Omega})$ (the so-called stored energy function) as

$$\mathbf{N} = \frac{\partial W}{\partial \boldsymbol{\Gamma}} \quad \text{and} \quad \mathbf{M} = \frac{\partial W}{\partial \boldsymbol{\Omega}} \ , \tag{2.11}$$

corresponding then to convected measures of the axial and transverse shear forces in $\mathbf{N}$, and bending and torsional moments in $\mathbf{M}$. The objectivity of these stress resultants follows easily from the frame indifference of the strain measures themselves. The numerical simulations presented in Sect. 5 consider the quadratic stored energy function

$$W(\boldsymbol{\Gamma}, \boldsymbol{\Omega}) = \tfrac{1}{2}\boldsymbol{\Gamma} \cdot \mathbb{C}_\Gamma \boldsymbol{\Gamma} + \tfrac{1}{2}\boldsymbol{\Omega} \cdot \mathbb{C}_\Omega \boldsymbol{\Omega} \ , \tag{2.12}$$

leading to the strain–stress relations

$$\mathbf{N} = \mathbb{C}_\Gamma \boldsymbol{\Gamma} \quad \text{and} \quad \mathbf{M} = \mathbb{C}_\Omega \boldsymbol{\Omega} \ , \tag{2.13}$$

linear in the strain measures. Typical elastic moduli for an isotropic elastic material homogeneous over the cross-section are given by the expressions

$$\mathbb{C}_\Gamma = \begin{bmatrix} GA_1 & 0 & 0 \\ 0 & GA_2 & 0 \\ 0 & 0 & EA \end{bmatrix}, \quad \text{and}$$

$$\mathbb{C}_\Omega = \begin{bmatrix} E\bar{\mathcal{I}}^{11} & E\bar{\mathcal{I}}^{12} & 0 \\ E\bar{\mathcal{I}}^{21} & E\bar{\mathcal{I}}^{22} & 0 \\ 0 & 0 & GJ \end{bmatrix} \ , \tag{2.14}$$

for the Young modulus E and the shear modulus G of the material, and the cross-section area A, the shear reduced areas A_α in the local directions $\mathbf{d}_\alpha^o$, the second moment of area $\bar{\mathcal{I}}^{\alpha\beta} = \int_{\mathcal{A}(S)} \left[\|\boldsymbol{\xi}\|^2 \delta^{\alpha\beta} - \xi^\alpha \xi^\beta \right] \mathrm{d}A$ and the torsional constant J of the reference cross-section, all based on standard arguments of strength of materials. We note, however, that the time-stepping algorithms developed in this work do not rely on this particular form of the elastic potential.

2.4 The rod's equations of motion

Given all the above considerations, the equations of motion of the rod can be written in weak form as

$$\int_0^L \left[A_{\rho_o} \dot{\mathbf{v}} \cdot \delta\mathbf{r} + \mathcal{I}_{\rho_o}^{\alpha\beta} \dot{\mathbf{v}}_\alpha \cdot \mathbf{v}_\beta + \mathbf{N} \cdot \delta\boldsymbol{\Gamma} + \mathbf{M} \cdot \delta\boldsymbol{\Omega} \right] \mathrm{d}S$$

$$= \int_0^L \left[\tilde{\mathbf{n}} \cdot \delta\mathbf{r} + \tilde{\mathbf{m}}^\alpha \cdot \delta\mathbf{d}_\alpha \right] \mathrm{d}S + \left[\bar{\mathbf{n}} \cdot \delta\mathbf{r} + \bar{\mathbf{m}}^\alpha \cdot \delta\mathbf{d}_\alpha \right]_{\Gamma_t}$$

$$\forall (\delta\mathbf{r}, \delta\mathbf{d}_1, \delta\mathbf{d}_2) \in TQ \ , \tag{2.15}$$

$$\int_0^L \left[A_{\rho_o} (\mathbf{v} - \dot{\mathbf{r}}) \cdot \delta\mathbf{v} + \mathcal{I}_{\rho_o}^{\alpha\beta} (\mathbf{v}_\alpha - \dot{\mathbf{d}}_\alpha) \cdot \delta\mathbf{v}_\beta \right] \mathrm{d}S = 0$$

$$\forall (\delta\mathbf{v}, \delta\mathbf{v}_1, \delta\mathbf{v}_2) \in T\mathcal{W} \ , \tag{2.16}$$

for the applied distributed loads $\tilde{\mathbf{n}}$ and moments $\tilde{\mathbf{m}}$ per unit of length in the undeformed configuration, and the applied loads $\bar{\mathbf{n}}$ and moments $\bar{\mathbf{m}}^\alpha$ at the boundary Γ_t. These equations are supplemented with the proper initial conditions, i.e., $\boldsymbol{\Phi}(S, 0) = \boldsymbol{\Phi}_o(S)$ and $\mathbf{W}(S, 0) = \mathbf{W}_o(S)$. We note again that summation over repeated indices is implied in (2.15) and (2.16).

Equation (2.15) corresponds to the weak statement of the balance of linear momentum, whereas (2.16) is a weak statement of the dynamic relations (2.2) defining the generalized velocities $\mathbf{v}$ and $\mathbf{v}_\alpha$ ($\alpha = 1, 2$). We observe that, in contrast with a more classical form of the equations in terms of the reduced angular velocity (2.3) [see e.g. Simo (1985)], the rotational terms have been expressed directly in terms of the directors and their rates. As first observed in Armero and Romero (2001c), this form of the equations leads naturally to the frame indifference of the finite element interpolations and to the proper conservation properties of the time-stepping schemes used in their integration. These equations will be the starting point of the dissipative numerical algorithms developed in the next section.

The admissible variations considered in the weak equations (2.15) and (2.16) belong to the tangent spaces TQ and $T\mathcal{W}$ of the configuration and velocity spaces (2.1) and (2.5), respectively. In particular, the linear space TQ has the same form as the velocity space (2.5), except for the imposed homogeneous boundary conditions on Γ_u (that is, $\delta\boldsymbol{\Phi} = 0$ on Γ_u). The admissible variations $\delta\boldsymbol{\Phi} = (\delta\mathbf{r}, \delta\mathbf{d}_1, \delta\mathbf{d}_2)_{\boldsymbol{\Phi}} \in \mathcal{W}_o$ can then be alternatively described by $\delta\tilde{\boldsymbol{\Phi}} = (\delta\mathbf{r}, \delta\boldsymbol{\theta})$ for the vector $\delta\boldsymbol{\theta} \in \mathbb{R}^3$ satisfying the relation

$$\delta\mathbf{d}_\alpha = \delta\boldsymbol{\theta}\times\mathbf{d}_\alpha, \quad \text{for } \alpha = 1,2\ . \tag{2.17}$$

In this way, the strain variations in (2.15) are given by

$$\delta\boldsymbol{\Gamma} = \boldsymbol{\Lambda}^{\mathrm{T}}(\delta\mathbf{r}_{,s} - \delta\boldsymbol{\theta}\times\mathbf{r}_{,s}) \quad \text{and} \quad \delta\boldsymbol{\Omega} = \boldsymbol{\Lambda}^{\mathrm{T}}\delta\boldsymbol{\theta}_{,s}\ , \tag{2.18}$$

as straightforward algebraic manipulations show.

The equivalence between these two possible parameterizations of the space of admissible variations is crucial for the developments presented later in this paper. To map one expression to the other, consider a variation in $T_{\boldsymbol{\Phi}}Q$ of the form $\delta\boldsymbol{\Phi} = (\delta\mathbf{r}, \delta\mathbf{d}_1, \delta\mathbf{d}_2, \delta\mathbf{d}_3)$, where the third director has been added to simplify the calculations, given by the expression

$$\delta\mathbf{d}_3 = \delta(\mathbf{d}_1\times\mathbf{d}_2) = \delta\mathbf{d}_1\times\mathbf{d}_2 + \mathbf{d}_1\times\delta\mathbf{d}_2 = \delta\boldsymbol{\theta}\times\mathbf{d}_3\ . \tag{2.19}$$

Then, observing the definition of the director variations (2.17), we can write the following relation between the two representations of the tangent vectors at $\boldsymbol{\Phi}$

$$\delta\boldsymbol{\Phi} = \begin{Bmatrix} \delta\mathbf{r} \\ \delta\mathbf{d}_1 \\ \delta\mathbf{d}_2 \\ \delta\mathbf{d}_3 \end{Bmatrix} = \boldsymbol{\Xi}(\boldsymbol{\Phi})\begin{Bmatrix} \delta\mathbf{r} \\ \delta\boldsymbol{\theta} \end{Bmatrix} = \boldsymbol{\Xi}(\boldsymbol{\Phi})\ \ \delta\tilde{\boldsymbol{\Phi}}\ . \tag{2.20}$$

The matrix $\boldsymbol{\Xi}(\boldsymbol{\Phi})$ expressing the change of parameterization of the tangent space is defined as

$$\boldsymbol{\Xi}(\boldsymbol{\Phi}) = \begin{bmatrix} \mathbf{1} & \mathbf{0} & \mathbf{0} & \mathbf{0} \\ \mathbf{0} & -\hat{\mathbf{d}}_1 & \mathbf{0} & \mathbf{0} \\ \mathbf{0} & \mathbf{0} & -\hat{\mathbf{d}}_2 & \mathbf{0} \\ \mathbf{0} & \mathbf{0} & \mathbf{0} & -\hat{\mathbf{d}}_3 \end{bmatrix}\ , \tag{2.21}$$

where we have denoted again by $\hat{\mathbf{d}}_\alpha$ the skew tensor with axial vector $\mathbf{d}_\alpha$ ($\alpha = 1,2$). The description of elements of TQ with vectors of the form $\delta\tilde{\boldsymbol{\Phi}}$ is more convenient for the numerical implementation, since there are no constraints on their components, its total number having been reduced from 12 to 6.

Similarly, the space of admissible velocity variations $T\mathcal{W}$, the tangent space of the velocity space $\mathcal{W}$, is given by the linear space

$$T\mathcal{W} = \{(\delta\mathbf{v}, \delta\mathbf{v}_1, \delta\mathbf{v}_2)_{\tilde{\mathbf{W}}=(\mathbf{v},\boldsymbol{\omega})} \ \text{ with, } \ \delta\mathbf{v}\in\mathbb{R}^3, \ \text{and} \\ \delta\mathbf{v}_\alpha = \delta\boldsymbol{\omega}\times\mathbf{d}_\alpha + \boldsymbol{\omega}\times\delta\mathbf{d}_\alpha, \ \text{ for } \quad \delta\boldsymbol{\omega}\in\mathbb{R}^3\}\ , \tag{2.22}$$

depending on the current configuration $\boldsymbol{\Phi}\in Q$ indirectly through its dependence on $\mathbf{W}\in\mathcal{W}$.

Remark 2.1. The above Lagrangian description of the governing equations in the velocity space is equivalent to a classical formulation of the canonical Hamilton's equations in the cotangent bundle T^*Q. This later form considers the associated momenta in the phase space T^*Q. The two forms of the equations are available thanks to the connection introduced by the inertias (2.7), defining

$$\mathbf{p} = A_{\rho_o}\mathbf{v} \quad \text{and} \quad \boldsymbol{\mu}^\alpha = \mathcal{I}^{\alpha\beta}_{\rho_o}\mathbf{v}_\beta\ , \tag{2.23}$$

for the translational and director momentum densities, respectively. We refer to Romero and Armero (2002a) for a complete discussion of these aspects, since the expression of the final equations directly on the director space is not standard.

2.5 The conservation laws

The mechanical system defined in the previous sections is a classical example of a Hamiltonian system and as such, it possesses several characteristic conservation laws under the proper assumptions on the boundary conditions and the loading. In this way, we consider the linear momentum $\mathbf{L}(t)$ and the angular momentum with respect to the origin $\mathbf{J}(t)$ of the rod, defined respectively as

$$\mathbf{L}(t) = \int_0^L A_{\rho_o}\mathbf{v}\,\mathrm{d}S \quad \text{and}$$

$$\mathbf{J}(t) = \int_0^L (A_{\rho_o}\mathbf{r}\times\mathbf{v} + \mathcal{I}^{\alpha\beta}_{\rho_o}\mathbf{d}_\alpha\times\mathbf{v}_\beta)\,\mathrm{d}S\ . \tag{2.24}$$

Assuming for simplicity, and without loss of generality, that no external work is applied to the system, the total energy $H(t)$ is defined as the sum of the kinetic energy $K(t)$ in (2.6) and the potential energy $V(t)$ as

$$\mathrm{H}(t) = \underbrace{\int_0^L \tfrac{1}{2}(A_{\rho_o}\mathbf{v}\cdot\mathbf{v} + \mathcal{I}^{\alpha\beta}_{\rho_o}\mathbf{v}_\alpha\cdot\mathbf{v}_\beta)\,\mathrm{d}S}_{K(t)} + \underbrace{\int_0^L W(\boldsymbol{\Gamma},\boldsymbol{\Omega})\,\mathrm{d}S}_{V(t)}\ , \tag{2.25}$$

defining at the same time the Hamiltonian function of the system.

Consider a system composed of a rod under external forces, subjected to boundary conditions $\boldsymbol{\Phi} = \bar{\boldsymbol{\Phi}}$ on Γ_u and initial conditions of position and velocity. Then the following conservation laws hold:

(i) If the sum of the external forces applied to the system is zero, the total linear momentum $(2.24)_1$ is constant, i.e., $\dot{\mathbf{L}} = \mathbf{0}$.
(ii) If the torque of the external forces with respect to the origin is zero, then the angular momentum $(2.24)_2$ is constant, i.e., $\dot{\mathbf{J}} = \mathbf{0}$.
(iii) If the total work applied by the external forces is zero, then the mechanical energy (2.25) is constant, i.e., $\dot{H} = 0$.

We refer again to Simo (1985) and Romero and Armero (2002a) for the proof of these conservation laws, the latter using again the direct parameterization of the governing equations directly in terms of the director fields and their variations, as it is employed in the numerical implementation considered next.

3
The spatial and temporal discretizations

We discuss in this section the spatial and temporal approximations of the variational equations of the rod problem. The spatial discretization is performed first through a standard finite element approximation. The resulting finite dimensional ordinary differential equations are approximated in time with a finite difference integrator designed to preserve linear and angular momenta and to allow a controllable, non-negative energy dissipation in the discrete solution.

3.1
The spatial finite element discretization

To formulate the Galerkin approximation of the variational problem (2.15), (2.16), finite dimensional subspaces of the functional spaces introduced in the previous section must be defined. To this purpose, a finite element mesh is constructed which partitions the rod axis in n_{el} one-dimensional elements connected at n_{node} nodes. Then, the configuration space, momentum space and their tangent spaces are approximated as

$$
\begin{aligned}
&Q \approx Q^h = \{\boldsymbol{\Phi}^h(S,t) = \sum_{A=1}^{n_{\text{node}}} N^A(S)\ \ \boldsymbol{\Phi}^A(t),\\
&\boldsymbol{\Phi}^A(t) = (\mathbf{r}^A(t), \mathbf{d}_1^A(t), \mathbf{d}_2^A(t)),\\
&\mathbf{r}^A(t) \in \mathbb{R}^3,\ \mathbf{d}_\alpha^A(t) \in S^2, \mathbf{d}_1^A \cdot \mathbf{d}_2^A = 0,\\
&\boldsymbol{\Phi}^A(t) = \bar{\boldsymbol{\Phi}}(S^A,t) \text{ for } A \in \Gamma_u\}\ ,
\end{aligned}
\tag{3.1}
$$

$$
\begin{aligned}
&TQ \approx TQ^h = \{\delta\boldsymbol{\Phi}^h(S) = \sum_{A=1}^{n_{\text{node}}} N^A(S)\ \ \delta\boldsymbol{\Phi}^A,\\
&\delta\boldsymbol{\Phi}^A = (\delta\mathbf{r}^A, \delta\mathbf{d}_1^A, \delta\mathbf{d}_2^A), \delta\mathbf{r}^A \in \mathbb{R}^3,\\
&\delta\mathbf{d}_\alpha^A = \delta\boldsymbol{\theta}^A \times \mathbf{d}_\alpha^A \quad \text{for } \alpha = 1,2\ ,\\
&\delta\boldsymbol{\Phi}^A = \mathbf{0} \text{ for } A \in \Gamma_u\}\ ,
\end{aligned}
\tag{3.2}
$$

$$
\begin{aligned}
&\mathcal{W} \approx \mathcal{W}^h = \{\mathbf{W}^h(S,t) = \sum_{A=1}^{n_{\text{node}}} N^A(S)\ \ \mathbf{W}^A(t)\ ,\\
&\mathbf{W}^A(t) = (\mathbf{v}^A(t), \mathbf{v}_1^A(t), \mathbf{v}_2^A(t))\ ,\\
&\mathbf{v}^A \in \mathbb{R}^3, \mathbf{v}_\alpha^A = \boldsymbol{\omega}^A \times \mathbf{d}_\alpha^A \quad \text{for } \alpha = 1,2\ \}\ ,
\end{aligned}
\tag{3.3}
$$

$$
\begin{aligned}
&T\mathcal{W} \approx T\mathcal{W}^h = \{\delta\mathbf{W}^h(S) = \sum_{A=1}^{n_{\text{node}}} N^A(S)\ \ \delta\mathbf{W}^A,\\
&\delta\mathbf{W}^A = (\delta\mathbf{v}^A, \delta\mathbf{v}_1^A, \delta\mathbf{v}_2^A)\ ,\\
&\delta\mathbf{W}^A \in \mathbb{R}^3 \times \mathbb{R}^3 \times \mathbb{R}^3\}\ ,
\end{aligned}
\tag{3.4}
$$

where $N^A(S)$ denotes a standard one–dimensional isoparametric shape function and $\boldsymbol{\Phi}^A$, $\delta\boldsymbol{\Phi}^A$, $\mathbf{W}^A$, $\delta\mathbf{W}^A$ are the nodal values of the configuration and velocity variables and their variations, respectively. As usual, the nodal variations do not depend on the time t in contrast with the nodal values of the configuration and velocity variables. The standard completeness conditions are assumed for the shape functions $N^A(S)$ (that is, the constant and linear functions are represented exactly). The Galerkin form of the problem is obtained by substituting the previous interpolations in the weak form (2.15), (2.16).

As indicated in the previous section, it is more convenient to parameterize the configuration variations in terms of the rotation vector variations $\delta\boldsymbol{\theta}$, through the introduction of the nodal values $\delta\boldsymbol{\theta}^A$. Using the mapping defined in Eq. (2.20), tangent vectors to the configuration space can be written as

$$
\begin{aligned}
\delta\boldsymbol{\Phi}^h(S) &= \sum_{A=1}^{n_{\text{node}}} N^A(S)\ \ \delta\boldsymbol{\Phi}^A(t)\\
&= \sum_{A=1}^{n_{\text{node}}} N^A(S)\ \ \boldsymbol{\Xi}(\boldsymbol{\Phi}^A)\delta\tilde{\boldsymbol{\Phi}}^A(t)\ .
\end{aligned}
\tag{3.5}
$$

We emphasize that the configuration variables $\boldsymbol{\Phi}$ and their variations $\delta\boldsymbol{\Phi}$ are interpolated in space S and not the reduced rotational parameters $\tilde{\boldsymbol{\Phi}}$ or their variations $\delta\tilde{\boldsymbol{\Phi}}$. This approximation imposes exactly the rotational character of the director motion (i.e., the directors are orthonormal) at the nodes only, but not necessarily inside the elements. Strictly speaking then, the finite dimensional spaces defined in (3.1)–(3.4) are not subsets of their infinite dimensional counterparts as required by the Galerkin's method, except in special cases. However, this "variational crime" is necessary for the frame indifference of the discrete model as first noted in Armero and Romero (2001c). Previous numerical implementations based on a finite element interpolation of the $\delta\tilde{\boldsymbol{\Phi}}$ or similar rotational parameters (see e.g. Simo (1985) and Cardona and Geradin (1989) among others), although imposing the rotational character of the interpolations pointwise, were noted to lack the required frame indifference in Crisfield and Jelenić (1998) and Jelenić and Crisfield (1999). Furthermore, the time-stepping algorithms based on these interpolations of the rotational parameters have been shown to lack the sought conserving properties. We refer to Romero and Armero (2002a) for complete details on all these issues, including an evaluation of the different approximations.

Remark 3.1. We observe also that the interpolations in $T\mathcal{W}^h$ is not consistent with their continuum definition (2.22) given the choice $\delta\mathbf{v}_\alpha \in \mathbb{R}^3$, as it is always tacitly assumed in the literature. This additional "variational crime" allows the algorithmic preservation of the desired conservation/dissipation properties.

3.2
The temporal discretization

The approximation of the variational problem (2.15), (2.16) is completed by the proper temporal discretization of the equations. As noted in Sect. 1, the goal here is that the final fully discrete system of equations (discrete in space and time) exhibits the conservation/dissipation properties of interest. To this purpose, we consider a partition of the interval of interest $[0,T]$ in $N+1$ points

$0 = t_0 < t_1 < \cdots < t_N = T$. Each pair of consecutive points defines a time step $[t_n, t_{n+1}]$ of length $\Delta t = t_{n+1} - t_n$, not necessarily constant. We denote the algorithmic approximation of any variable, say, $\mathbf{y}$ at time t_n and t_{n+1} by $\mathbf{y}_n$ and $\mathbf{y}_{n+1}$, respectively. We also make use of the convex combination $\mathbf{y}_{n+\vartheta} = (1-\vartheta)\mathbf{y}_n + \vartheta \mathbf{y}_{n+1}$ for any $\vartheta \in [0,1]$.

With this notation at hand, we consider the discretization of the governing equations (2.15) and (2.16) given by

$$\begin{aligned}\int_0^L \Big[A_{\rho_o} \frac{\mathbf{v}^h_{n+1} - \mathbf{v}^h_n}{\Delta t} \cdot \delta \mathbf{r}^h + \mathcal{I}^{\alpha\beta}_{\rho_o} \frac{\mathbf{v}^h_{\alpha,n+1} - \mathbf{v}^h_{\alpha,n}}{\Delta t} \cdot \delta \mathbf{v}^h_\beta + \mathbf{N}^* \cdot \delta \boldsymbol{\Gamma}_* \\ + \mathbf{M}^* \cdot \delta \boldsymbol{\Omega}_* \Big] dS = \int_0^L \Big[\tilde{\mathbf{n}}_{n+\frac{1}{2}} \cdot \delta \mathbf{r}^h + \tilde{\mathbf{m}}^\alpha_{n+\frac{1}{2}} \cdot \delta \mathbf{d}^h_\alpha \Big] dS \\ + \Big[\bar{\mathbf{n}}_{n+\frac{1}{2}} \cdot \delta \mathbf{r}^h + \bar{\mathbf{m}}^\alpha_{n+\frac{1}{2}} \cdot \delta \mathbf{d}^h_\alpha \Big]_{\Gamma_t} \quad \forall (\delta \mathbf{r}^h, \delta \mathbf{d}^h_1, \delta \mathbf{d}^h_2) \in TQ^h \ , \end{aligned} \tag{3.6}$$

$$\int_0^L \Big[A_{\rho_o} \Big(\mathbf{v}^* - \frac{\mathbf{r}^h_{n+1} - \mathbf{r}^h_n}{\Delta t} \Big) \cdot \delta \mathbf{v}^h + \mathcal{I}^{\alpha\beta}_{\rho_o} \Big(\mathbf{v}^*_\alpha - \frac{\mathbf{d}^h_{\alpha,n+1} - \mathbf{d}^h_{\alpha,n}}{\Delta t} \Big) \cdot \delta \mathbf{v}^h_\beta \Big] dS = 0 \quad \forall (\delta \mathbf{v}^h, \delta \mathbf{v}^h_1, \delta \mathbf{v}^h_2) \in T\mathcal{W}^h \ , \tag{3.7}$$

in combination with the spatial finite element discretizations considered in the previous section, as denoted by the superscript $(\cdot)^h$. The Eqs. (3.6) and (3.7) consider a difference quotient for the time derivatives in the original continuum equations (2.15) and (2.16) and, consistent with the developments that follow, the evaluation of the applied loading has been considered at the mid–point $t_{n+\frac{1}{2}} = (t_n + t_{n+1})/2$. It remains to define the approximation of the strain variations, the stress resultants and velocities, all marked with an asterisk in the equations (3.6) and (3.7). Their precise definitions are obtained by imposing the desired conservation/dissipation properties of the final scheme.

In this way, and as shown in Proposition 3.1 below, a momentum conserving scheme is obtained by considering the strain variations based on the mid-point configuration $\boldsymbol{\Phi}^h_{n+1/2} = \frac{1}{2}(\boldsymbol{\Phi}^h_n + \boldsymbol{\Phi}^h_{n+1})$, that is, in terms of the nodal variations

$$\begin{aligned}\delta \boldsymbol{\Phi}^A &= (\delta \mathbf{r}^A, \delta \mathbf{d}^A_1, \delta \mathbf{d}^A_2) \quad \text{with } \delta \mathbf{d}^A_\alpha \\ &= \delta \boldsymbol{\theta}^A \times \mathbf{d}^A_{\alpha,n+1/2} \quad \text{for } \alpha = 1,2 \ , \end{aligned} \tag{3.8}$$

where $\delta \mathbf{r}^A \in \mathbb{R}^3$, $\delta \boldsymbol{\theta}^A \in \mathbb{R}^3$ and $\mathbf{d}^A_{\alpha,n+1/2} = \frac{1}{2}(\mathbf{d}^A_{\alpha,n} + \mathbf{d}^A_{\alpha,n+1})$. Equivalently, we can write in the compact form introduced in Eq. (2.20) the relation

$$\delta \boldsymbol{\Phi}^A = \boldsymbol{\Xi}^A_{n+1/2} \delta \tilde{\boldsymbol{\Phi}}^A \ , \tag{3.9}$$

with $\boldsymbol{\Xi}^A_{n+1/2} = \frac{1}{2}(\boldsymbol{\Xi}(\boldsymbol{\Phi}^A_n) + \boldsymbol{\Xi}(\boldsymbol{\Phi}^A_{n+1}))$ and $\delta \tilde{\boldsymbol{\Phi}}^A = (\delta \mathbf{r}^A, \delta \boldsymbol{\theta}^A) \in \mathbb{R}^3 \times \mathbb{R}^3$.

Given the finite element interpolations introduced in the previous section, the strain variations (2.18) read

$$\begin{aligned}\left\{ \begin{array}{c} \delta \boldsymbol{\Gamma}_* \\ \delta \boldsymbol{\Omega}_* \end{array} \right\} &= \sum_{A=1}^{n_{\text{node}}} \mathbb{B}^A_{n+1/2} \delta \boldsymbol{\Phi}^A \\ &= \sum_{A=1}^{n_{\text{node}}} \mathbb{B}^A_{n+1/2} \boldsymbol{\Xi}^A_{n+1/2} \delta \tilde{\boldsymbol{\Phi}}^A \ , \end{aligned} \tag{3.10}$$

in terms of the linearized strain operator $\mathbb{B}^A_{n+1/2} = \frac{1}{2}(\mathbb{B}^A_n + \mathbb{B}^A_{n+1})$. Each one of the matrices $\mathbb{B}_n$, $\mathbb{B}_{n+1}$ is defined as

$$\mathbb{B}^A = \begin{bmatrix} N^A_{,s} \mathbf{d}^{h\mathrm{T}}_1 & N^A \mathbf{r}^{h\mathrm{T}}_{,s} & \mathbf{0}^{\mathrm{T}} & \mathbf{0}^T \\ N^A_{,s} \mathbf{d}^{h\mathrm{T}}_2 & \mathbf{0}^{\mathrm{T}} & N^A \mathbf{r}^{h\mathrm{T}}_{,s} & \mathbf{0}^{\mathrm{T}} \\ N^A_{,s} \mathbf{d}^{h\mathrm{T}}_3 & \mathbf{0}^{\mathrm{T}} & \mathbf{0}^{\mathrm{T}} & N^A \mathbf{r}^{h\mathrm{T}}_{,s} \\ \mathbf{0}^{\mathrm{T}} & \mathbf{0}^{\mathrm{T}} & \frac{1}{2}(N^A_{,s} \mathbf{d}^h_3 - N^A \mathbf{d}^h_{3,s}) & \frac{1}{2}(N^A_{,s} \mathbf{d}^h_2 - N^A \mathbf{d}^h_{2,s}) \\ \mathbf{0}^{\mathrm{T}} & \frac{1}{2}(N^A_{,s} \mathbf{d}^h_3 - N^A \mathbf{d}^h_{3,s}) & \mathbf{0}^T & \frac{1}{2}(N^A_{,s} \mathbf{d}^h_1 - N^A \mathbf{d}^h_{1,s}) \\ \mathbf{0}^{\mathrm{T}} & \frac{1}{2}(N^A_{,s} \mathbf{d}^h_2 - N^A \mathbf{d}^h_{2,s}) & \frac{1}{2}(N^A_{,s} \mathbf{d}^h_1 - N^A \mathbf{d}^h_{1,s}) & \mathbf{0}^T \end{bmatrix} \ , \tag{3.11}$$

where the vector terms are evaluated at the corresponding time instant t_n or t_{n+1}, respectively. This expression follows after expanding the strain variations directly in terms of the variations of the directors rather than the reduced variation vector in (2.18). The general expanded expression of the strain measures (2.9) is employed to this purpose. Details are omitted. As noted in the previous section, the direct interpolation of the directors instead of the reduced rotational parameters is crucial for the frame indifference of the final discrete formulation.

Of interest here is the evolution of the total momenta of the discrete dynamical system, defined by the very same continuum relations (2.24) but now involving the interpolated finite element variables (3.1) and (3.3). With the approximations of the strain variations (3.10) at hand, the following result holds:

Proposition 3.1 The fully discrete system of equations (3.6) and (3.7) with the strain variations (3.10) preserves the conservation laws of linear and angular momentum of the continuum system stated in Sect. 2.5, the latter if the vectors $\mathbf{v}^*$, $\mathbf{v}^*_1$ and $\mathbf{v}^*_2$ approximating the generalized velocities satisfy the relations

$$\mathbf{v}^* \times \mathbf{v}^h_{n+\frac{1}{2}} = 0 \quad \text{and} \quad \mathcal{I}^{\alpha\beta}_{\rho_o} \mathbf{v}^*_\alpha \times \mathbf{v}^h_{\beta,n+\frac{1}{2}} = 0 \ , \tag{3.12}$$

(summation implied in this last relation, as usual) for the mid-point values $\mathbf{v}^h_{n+\frac{1}{2}}$, $\mathbf{v}^h_{1,n+\frac{1}{2}}$ and $\mathbf{v}^h_{2,n+\frac{1}{2}}$.

Proof: To prove the conservation of linear momentum, we consider the variations

$$(\delta\mathbf{r}^h, \delta\mathbf{d}_1^h, \delta\mathbf{d}_2^h) = (\mathbf{c}, \mathbf{0}, \mathbf{0}) \in TQ^h \ , \tag{3.13}$$

for a constant $\mathbf{c} \in \mathbb{R}^3$ in the discrete weak equilibrium equation (3.6). We observe that the constant vectors (3.13) define indeed admissible variations given the assumed completeness of the shape functions defining the finite element interpolations. By assumption, the terms involving the external forces are zero and it is easily verified that the strain variations also vanish. The only remaining terms in the weak equilibrium equation are the inertial terms, leading to the relation

$$\begin{aligned} 0 &= \int_0^L A_{\rho_o} \frac{\mathbf{v}_{n+1}^h - \mathbf{v}_n^h}{\Delta t} \cdot \mathbf{c}\, \mathrm{d}S = \frac{\mathbf{c}}{\Delta t} \cdot \int_0^L A_{\rho_o} \big(\mathbf{v}_{n+1}^h - \mathbf{v}_n^h\big) \mathrm{d}S \\ &= \frac{\mathbf{c}}{\Delta t} \cdot \big(\mathbf{L}_{n+1}^h - \mathbf{L}_n^h\big) \ , \end{aligned} \tag{3.14}$$

for all $\mathbf{c} \in \mathbb{R}^3$. Hence, we conclude that $\mathbf{L}_{n+1}^h = \mathbf{L}_n^h$ proving the result for the conservation law of the linear momentum.

To prove the conservation of angular momentum, we consider the variations

$$\begin{aligned} &(\delta\mathbf{r}^h, \delta\mathbf{d}_1^h, \delta\mathbf{d}_2^h) \\ &\quad = (\mathbf{c} \times \mathbf{r}_{n+1/2}^h, \mathbf{c} \times \mathbf{d}_{1,n+1/2}^h, \mathbf{c} \times \mathbf{d}_{2,n+1/2}^h) \in TQ^h \ , \end{aligned} \tag{3.15}$$

and

$$\begin{aligned} &(\delta\mathbf{v}^h, \delta\mathbf{v}_1^h, \delta\mathbf{v}_2^h) \\ &\quad = (\mathbf{c} \times \mathbf{v}_{n+1/2}^h, \quad , \mathbf{c} \times \mathbf{v}_{1,n+1/2}^h, \mathbf{c} \times \mathbf{v}_{2,n+1/2}^h) \in T\mathcal{W}^h \ , \end{aligned} \tag{3.16}$$

in the discrete governing equations (3.6) and (3.7), respectively, for an arbitrary constant vector $\mathbf{c} \in \mathbb{R}^3$. Note that the director variations belong to the correct director tangent space, given in terms of the associated nodal values. As before, the terms involving external forces are zero by assumption and the strain variations (3.10) vanish again for this particular choice of configuration variations, as a straightforward calculation shows. The rest of the weak equation (3.6) reads

$$\begin{aligned} 0 &= \int_0^L \left[A_{\rho_o} \frac{\mathbf{v}_{n+1}^h - \mathbf{v}_n^h}{\Delta t} \cdot \left(\mathbf{c} \times \mathbf{r}_{n+\frac{1}{2}}^h \right) \right. \\ &\quad \left. + \mathcal{I}_{\rho_o}^{\alpha\beta} \frac{\mathbf{v}_{\alpha,n+1}^h - \mathbf{v}_{\alpha,n}^h}{\Delta t} \cdot \left(\mathbf{c} \times \mathbf{d}_{\beta,n+1/2}^h \right) \right] \mathrm{d}S \\ &= \frac{\mathbf{c}}{\Delta t} \cdot \int_0^L \Big[\Big(A_{\rho_o} \mathbf{r}_{n+1}^h \times \mathbf{v}_{n+1}^h + \mathcal{I}_{\rho_o}^{\alpha\beta} \mathbf{d}_{\alpha,n+1}^h \times \mathbf{v}_{\beta,n+1}^h \Big) \\ &\quad - \Big(A_{\rho_o} \mathbf{r}_n^h \times \mathbf{v}_n^h + \mathcal{I}_{\rho_o}^{\alpha\beta} \mathbf{d}_{\alpha,n}^h \times \mathbf{v}_{\beta,n}^h \Big) \Big] \mathrm{d}S \\ &\quad - \int_0^L \left[A_{\rho_o} \frac{\mathbf{r}_{n+1}^h - \mathbf{r}_n^h}{\Delta t} \cdot \left(\mathbf{c} \times \mathbf{v}_{n+\frac{1}{2}}^h \right) \right. \\ &\quad \left. + \mathcal{I}_{\rho_o}^{\alpha\beta} \frac{\mathbf{d}_{\alpha,n+1}^h - \mathbf{d}_{\alpha,n}^h}{\Delta t} \cdot \left(\mathbf{c} \times \mathbf{v}_{\beta,n+\frac{1}{2}}^h \right) \right] \mathrm{d}S \\ &= \frac{\mathbf{c}}{\Delta t} \cdot (\mathbf{J}_{n+1}^h - \mathbf{J}_n^h) \\ &\quad - \mathbf{c} \cdot \int_0^L \left[A_{\rho_o} \mathbf{v}^* \times \mathbf{v}_{n+\frac{1}{2}}^h + \mathcal{I}_{\rho_o}^{\alpha\beta} \mathbf{v}_\alpha^* \times \mathbf{v}_{\beta,n+\frac{1}{2}}^h \right] \mathrm{d}S \ \text{(by (3.7))} \\ &= \frac{\mathbf{c}}{\Delta t} \cdot (\mathbf{J}_{n+1}^h - \mathbf{J}_n^h) \ , \end{aligned} \tag{3.17}$$

the last equality following by the assumed conditions (3.12) in the statement of the proposition. Since the vector $\mathbf{c}$ is again arbitrary, the conservation of the angular momentum in the time step (i.e., $\mathbf{J}_{n+1} = \mathbf{J}_n$) follows, proving the proposition.

3.3 Energy consistent approximations of the stress resultants and velocities

It remains to define the temporal approximations of the stress resultants $\mathbf{N}^*$ and $\mathbf{M}^*$, and the velocities $\mathbf{v}^*$ and $\mathbf{v}_\alpha^*$, the latter satisfying the conditions (3.12) for the discrete system to inherit the conservation law of angular momenta. As discussed in Section 1, it is our goal to define these approximations such that the final discrete dynamical system exhibits a controllable, unconditionally non-negative numerical energy dissipation, with full energy conservation as a particular case.

To this purpose, we investigate first the evolution of the energy along the solutions of the discrete system. This evolution can be obtained by introducing the variations

$$\begin{aligned} (\delta\mathbf{r}^h, \delta\mathbf{d}_1^h, \delta\mathbf{d}_2^h) &= (\mathbf{r}_{n+1}^h - \mathbf{r}_n^h, \mathbf{d}_{1,n+1}^h - \mathbf{d}_{1,n}^h, \mathbf{d}_{2,n+1}^h - \mathbf{d}_{2,n}^h) \\ &= \mathbf{\Phi}_{n+1}^h - \mathbf{\Phi}_n^h \ \in \ TQ^h \ , \\ (\delta\mathbf{v}^h, \delta\mathbf{v}_1^h, \delta\mathbf{v}_2^h) &= (\mathbf{v}_{n+1}^h - \mathbf{v}_n^h, \mathbf{v}_{1,n+1}^h - \mathbf{v}_{1,n}^h, \mathbf{v}_{2,n+1}^h - \mathbf{v}_{2,n}^h) \\ &= \mathbf{W}_{n+1}^h - \mathbf{W}_n^h \ \in T\mathcal{W}^h \ , \end{aligned} \tag{3.18}$$

in the discrete governing equations. We observe that these variations are indeed admissible (i.e. they belong to the spaces indicated in (3.18)) through the corresponding nodal values, and that they correspond to the increments of the configuration and velocity variables in the time step of interest. The corresponding discrete strain variations, given by (3.10), are

$$\begin{aligned} \left\{ \begin{array}{c} \delta\mathbf{\Gamma}_* \\ \delta\mathbf{\Omega}_* \end{array} \right\} &= \sum_{A=1}^{n_{\text{node}}} \mathbb{B}_{n+1/2}^A \big(\mathbf{\Phi}_{n+1}^A - \mathbf{\Phi}_n^A \big) \\ &= \left\{ \begin{array}{c} \mathbf{\Gamma}_{n+1}^h - \mathbf{\Gamma}_n^h \\ \mathbf{\Omega}_{n+1}^h - \mathbf{\Omega}_n^h \end{array} \right\} \ , \end{aligned} \tag{3.19}$$

that is, the increment of the discrete strain measures, as an algebraic calculation shows. We note that this result does not depend on the pointwise orthogonality of directors,

thanks to the general definition (2.9) of the discrete strains.

Inserting these variations in the discrete governing equations (3.6) and (3.7), we obtain after adding the resulting expressions in the case of interest with no external work

$$\int_0^L \left[\mathbf{N}^* \cdot \left(\mathbf{\Gamma}^h_{n+1} - \mathbf{\Gamma}^h_n\right) + \mathbf{M}^* \cdot \left(\mathbf{\Omega}^h_{n+1} - \mathbf{\Omega}^h_n\right)\right] \mathrm{d}S + \int_0^L \left[\mathbf{v}^* \cdot A_{\rho_o}\left(\mathbf{v}^h_{n+1} - \mathbf{v}^h_n\right) + \mathbf{v}^*_\alpha \cdot \mathcal{I}^{\alpha\beta}_{\rho_o}\left(\mathbf{v}^h_{\beta,n+1} - \mathbf{v}^h_{\beta,n}\right)\right] \mathrm{d}S = 0 \ , \tag{3.20}$$

showing the energy evolution in the discrete system. The first term in this equality can be identified as the work done by the stress resultants $\mathbf{N}^*$ and $\mathbf{M}^*$ on the increments of the associated strains, whereas the second term measures the change of kinetic energy associated with the velocity approximations $\mathbf{v}^*$ and $\mathbf{v}^*_\alpha$.

Since our goal is the formulation of dissipative approximations of the governing equations, with a controllable numerical dissipation including, in particular, the energy conserving case, we consider the additive splits

$$\mathbf{N}^* = \mathbf{N}_{\text{cons}} + \mathbf{N}_{\text{diss}}, \quad \mathbf{M}^* = \mathbf{M}_{\text{cons}} + \mathbf{M}_{\text{diss}} \ , \tag{3.21}$$

and

$$\mathbf{v}^* = \mathbf{v}_{\text{cons}} + \mathbf{v}_{\text{diss}}, \quad \mathbf{v}^*_\alpha = \mathbf{v}_{\alpha,\text{cons}} + \mathbf{v}_{\alpha,\text{diss}} \ \ (\alpha = 1, 2) \ , \tag{3.22}$$

in conservative and dissipative parts of the approximations of the stress resultants and velocities, respectively. The conserving parts of the stress resultants are defined by the relation

$$\mathbf{N}_{\text{cons}} \cdot \left(\mathbf{\Gamma}^h_{n+1} - \mathbf{\Gamma}^h_n\right) + \mathbf{M}_{\text{cons}} \cdot \left(\mathbf{\Omega}^h_{n+1} - \mathbf{\Omega}^h_n\right) = W_{n+1} - W_n \tag{3.23}$$

that is, resulting in the change of the strain energy $W_{n+i} = W(\mathbf{\Gamma}^h_{n+i}, \mathbf{\Omega}^h_{n+i})$ $(i = 0, 1)$, with the conserving part of the velocity approximations defined by the relation

$$\mathbf{v}_{\text{cons}} \cdot A_{\rho_o}\left(\mathbf{v}^h_{n+1} - \mathbf{v}^h_n\right) + \mathbf{v}_{\alpha,\text{cons}} \cdot \mathcal{I}^{\alpha\beta}_{\rho_o}\left(\mathbf{v}^h_{\beta,n+1} - \mathbf{v}^h_{\beta,n}\right) = \mathcal{K}_{\rho_o n+1} - \mathcal{K}_{\rho_o n} \ , \tag{3.24}$$

for the kinetic energy density $\mathcal{K}_{\rho_o n+i}(\mathbf{v}^h_{n+i}, \mathbf{v}^h_{1,n+i}, \mathbf{v}^h_{2,n+i})$ $(i = 0, 1)$ defined in (2.6). On the other hand, the dissipaive parts are defined such that the relations

$$\mathbf{N}_{\text{diss}} \cdot \left(\mathbf{\Gamma}^h_{n+1} - \mathbf{\Gamma}^h_n\right) + \mathbf{M}_{\text{diss}} \cdot \left(\mathbf{\Omega}^h_{n+1} - \mathbf{\Omega}^h_n\right) = \mathcal{D}_W \tag{3.25}$$

and

$$\mathbf{v}_{\text{cons}} \cdot A_{\rho_o}\left(\mathbf{v}^h_{n+1} - \mathbf{v}^h_n\right) + \mathbf{v}_{\alpha,\text{cons}} \cdot \mathcal{I}^{\alpha\beta}_{\rho_o}\left(\mathbf{v}^h_{\beta,n+1} - \mathbf{v}^h_{\beta,n}\right) = \mathcal{D}_K \ , \tag{3.26}$$

are satisfied for different local density functions $\mathcal{D}_W$ and $\mathcal{D}_K$ to be defined.

Combining relations (3.23) to (3.26) with the energy evolution relation (3.20), we obtain the final relation

$$H^h_{n+1} - H^h_n = -\underbrace{\int_0^L (\mathcal{D}_W + \mathcal{D}_K)\, \mathrm{d}S}_{\mathcal{D}} \ , \tag{3.27}$$

identifying the evolution of the total energy of the discrete system

$$H^h_{n+i} := \int_0^L \left[\tfrac{1}{2}\mathbf{v}^h_{n+i} \cdot A_{\rho_o}\mathbf{v}^h_{n+i} + \tfrac{1}{2}\mathbf{v}^h_{\alpha,n+i} \cdot \mathcal{I}^{\alpha\beta}_{\rho_o}\mathbf{v}^h_{\beta,n+i} + W(\mathbf{\Gamma}^h_{n+i}, \mathbf{\Omega}^h_{n+i})\right] \mathrm{d}S \ , \tag{3.28}$$

for $i = 0, 1$. Clearly, the interest here is the definition of the dissipative part of the stress and velocity approximations such that the total numerical dissipation is non-negative, that is, $\mathcal{D} \geq 0$.

For the linear strain–stress relations (2.13), the conserving part of the stress resultants is easily obtained as

$$\mathbf{N}_{\text{cons}} = \mathbb{C}_\Gamma \tfrac{1}{2}\left(\mathbf{\Gamma}^h_n + \mathbf{\Gamma}^h_{n+1}\right) \quad \text{and}$$
$$\mathbf{M}_{\text{cons}} = \mathbb{C}_\Omega \tfrac{1}{2}\left(\mathbf{\Omega}^h_n + \mathbf{\Omega}^h_{n+1}\right) \ , \tag{3.29}$$

with (3.23) leading trivially to the difference of the quadratic potential (2.12). Similarly, given the quadratic character of the kinetic energy density $\mathcal{K}_{\rho_o}$ (2.6) in the velocities, the conserving part of the velocities can be easily expressed as

$$\mathbf{v}_{\text{cons}} = \mathbf{v}^h_{n+\frac{1}{2}} \quad \text{and} \quad \mathbf{v}_{\alpha,\text{cons}} = \mathbf{v}^h_{\alpha,n+\frac{1}{2}} \ \ (\alpha = 1, 2) \ , \tag{3.30}$$

for the corresponding mid-point values. We observe that the conditions (3.12), identified in Proposition 3.1 as necessary for the conservation of angular momentum, are satisfied with the choice (3.30). In particular, the relation $(3.12)_2$ for the director velocity follows from the symmetry of the dyadic $\mathcal{I}^{\alpha\beta}_{\rho_o}$ and the skew-symmetry of the combination $\mathbf{v}^h_{\alpha,n+\frac{1}{2}} \times \mathbf{v}^h_{\beta,n+\frac{1}{2}}$ in the indices $\{\alpha, \beta\}$. Extensions of the conserving approximations (3.29) to non-quadratic potentials $W(\cdot)$ can be easily obtained using the formalism proposed in González (2000); details are omitted here.

The modified mid-point evaluations (3.29) for the stress resultants were first proposed in Simo et al. (1995) in the current context of Cosserat rods but, as noted in Romero and Armero (2002a), the conserving character of the final fully discrete approximation depends crucially on the direct interpolation of the director fields (3.1) leading to the mid-point evaluation of the director velocity (3.30) instead of the angular velocity (2.3) associated to the reduced rotational parameters. In this way, the numerical schemes proposed in Simo et al. (1995) not only lack frame-indifference but also the energy conserving property in contrast with the conserving scheme considered here, a scheme first proposed in Armero and Romero (2001c). The challenge in this paper is the formulation of extensions that accommodate a controllable energy dissipation through the dissipative contributions in (3.21) and (3.22), as we develop in the following section.

3.4
Energy dissipative schemes

It remains to define the dissipative parts of the stress resultants and velocities in (3.21) and (3.22) satisfying the relations (3.25) and (3.26), respectively, determining in the process the dissipation functions $\mathcal{D}_W$ and $\mathcal{D}_K$. Motivated by these relations we write these dissipative parts as

$$\mathbf{N}_{\text{diss}} = \frac{\mathcal{D}_\Gamma}{\|\boldsymbol{\Gamma}^h_{n+1} - \boldsymbol{\Gamma}^h_n\|_{\mathsf{C}_\Gamma}} \frac{\mathbb{C}_\Gamma(\boldsymbol{\Gamma}^h_{n+1} - \boldsymbol{\Gamma}^h_n)}{\|\boldsymbol{\Gamma}^h_{n+1} - \boldsymbol{\Gamma}^h_n\|_{\mathsf{C}_\Gamma}} \ , \tag{3.31}$$

and

$$\mathbf{M}_{\text{diss}} = \frac{\mathcal{D}_\Omega}{\|\boldsymbol{\Omega}^h_{n+1} - \boldsymbol{\Omega}^h_n\|_{\mathsf{C}_\Omega}} \frac{\mathbb{C}_\Omega(\boldsymbol{\Omega}^h_{n+1} - \boldsymbol{\Omega}^h_n)}{\|\boldsymbol{\Omega}^h_{n+1} - \boldsymbol{\Omega}^h_n\|_{\mathsf{C}_\Omega}} \ , \tag{3.32}$$

in terms of two dissipation functions $\mathcal{D}_\Gamma$ and $\mathcal{D}_\Omega$ associated to the axial/shear forces and bending/torsional moments, respectively. The particular case given by the relations (2.13) has been assumed when writing the expressions (3.31) and (3.32) although, as noted in Remark 3.2 below, these expressions apply also to the general case for any other (non-quadratic) elastic potential. Here, the symbols $\|\cdot\|_{\mathsf{C}}$ denote the weighted Euclidean norms

$$\|\boldsymbol{\Gamma}\|^2_{\mathsf{C}_\Gamma} := \boldsymbol{\Gamma} \cdot \mathbb{C}_\Gamma \boldsymbol{\Gamma} \ , \quad \text{and} \quad \|\boldsymbol{\Omega}\|^2_{\mathsf{C}_\Omega} := \boldsymbol{\Omega} \cdot \mathbb{C}_\Omega \boldsymbol{\Omega} \ , \tag{3.33}$$

using the assumed positive definiteness of the tangent moduli (2.14); see again Remark 3.2 otherwise.

From (3.25), we conclude that

$$\mathcal{D}_W = \mathcal{D}_\Gamma + \mathcal{D}_\Omega \ . \tag{3.34}$$

Clearly, the motivation behind the definitions (3.31) and (3.32) is, given (3.25), the introduction of the dissipations $\mathcal{D}_\Gamma$ and $\mathcal{D}_\Omega$ along the direction of the increments of the corresponding strain measures. Obviously, a general formula can be considered accommodating a contribution in the orthogonal direction in the metric defined by the tangent moduli $\mathbb{C}_\Gamma$ and $\mathbb{C}_\Omega$. The challenge here is in the definition of the dissipation functions $\mathcal{D}_\Gamma$ and $\mathcal{D}_\Omega$ that lead to consistent approximations of the stress resultants and to a non-negative controllable energy dissipation. In particular, they must satisfy the limit relations

$$\begin{aligned} &\mathcal{D}_\Gamma \to 0 \quad \text{as} \quad \boldsymbol{\Gamma}^h_{n+1} \to \boldsymbol{\Gamma}^h_n, \quad \text{and} \\ &\mathcal{D}_\Omega \to 0 \quad \text{as} \quad \boldsymbol{\Omega}^h_{n+1} \to \boldsymbol{\Omega}^h_n \ , \end{aligned} \tag{3.35}$$

given the quotient in (3.31) and (3.32), for a well-defined stress approximation. The flexibility of the approach proposed here, allowing the introduction of this dissipation through the different components of the stress response (i.e., axial/shear forces or bending/torsional moments) is to be noted.

The choice of the dissipative part of the velocity approximations $\mathbf{v}^*$ and $\mathbf{v}^*_\alpha$ follows similar arguments, but now constrained by the relations (3.12) so the conservation law of angular momentum is preserved. This last requirement is accomplished by setting these vectors parallel to the mid–point values $\mathbf{v}^h_{n+\frac{1}{2}}$ and $\mathbf{v}^h_{\alpha,n+\frac{1}{2}}$, respectively, as occurred with the conserving contributions discussed in the previous section. In this way, we consider the approximations

$$\mathbf{v}_{\text{diss}} = \frac{\mathcal{D}_v}{v_{n+1} - v_n} \frac{\mathbf{v}^h_n + \mathbf{v}^h_{n+1}}{v_{n+1} + v_n} \ , \quad \text{and}$$

$$\mathbf{v}_{\alpha,\text{diss}} = \frac{\mathcal{D}_v}{v_{n+1} - v_n} \frac{\mathbf{v}^h_{\alpha,n} + \mathbf{v}^h_{\alpha,n+1}}{v_{n+1} + v_n} \ , \tag{3.36}$$

where we have introduced the notation

$$v_{n+i} \equiv \|\mathbf{v}^h_{n+i}\| := \sqrt{\mathbf{v}^h_{n+i} \cdot \mathbf{v}^h_{n+i}} \tag{3.37}$$

and

$$v_{n+i} \equiv \|(\mathbf{v}^h_{1,n+i}, \mathbf{v}^h_{2,n+i})\|_{\mathcal{I}_{\rho_o}/A_{\rho_o}} := \sqrt{\mathbf{v}^h_{\alpha,n+i} \cdot \frac{\mathcal{I}^{\alpha\beta}_{\rho_o}}{A_{\rho_o}} \mathbf{v}^h_{\beta,n+i}} \ , \tag{3.38}$$

for $i = 0, 1$, that is, the norms of the translational velocity and the rotational velocities, respectively, the latter weighted by the (positive definite) inertia introduced in (2.7). We note that both v_{n+i} and v_{n+i} have units of velocity (space/time).

As occurred with the dissipative part of the stress resultants in (3.31) and (3.32), we consider the dissipative part of the velocity approximations explicitly in terms of two different numerical dissipation density functions $\mathcal{D}_v$ and $\mathcal{D}_v$ associated to the translational and director velocities, respectively. In fact, introducing the formulas (3.36) in the relation (3.26), we obtain

$$\mathcal{D}_K = \mathcal{D}_v + \mathcal{D}_v \ , \tag{3.39}$$

for the function $\mathcal{D}_K$. The limit relations

$$\begin{aligned} &\mathcal{D}_v \to 0 \ \text{ as } v_{n+1} \to v_n, \quad \text{and} \\ &\mathcal{D}_v \to 0 \ \text{ as } v_{n+1} \to v_n \ , \end{aligned} \tag{3.40}$$

need to be imposed for well-defined expressions (3.36) as occurred in the approximations of the stress resultants.

Hence, with all these considerations, the total numerical dissipation (3.27) introduced by the numerical scheme reads as

$$H^h_{n+1} - H^h_n = -\underbrace{\int_0^L \Big(\underbrace{\mathcal{D}_\Gamma + \mathcal{D}_\Omega}_{\mathcal{D}_W} + \underbrace{\mathcal{D}_v + \mathcal{D}_v}_{\mathcal{D}_K} \Big) \, \mathrm{d}S}_{\mathcal{D}} \ . \tag{3.41}$$

Remarkably, we have reduced the problem to the definition of four scalar values ($\mathcal{D}_\Gamma$, $\mathcal{D}_\Omega$, $\mathcal{D}_v$ and $\mathcal{D}_v$) locally, that is, at each quadrature point in a typical finite element implementation as elaborated further in the following section. We note that these values appear under an integral sign, whose evaluation is then needed at this level of quadrature points. Clearly, we need to impose the requirement $\mathcal{D} \geq 0$ unconditionally, not necessarily each of the four components of the numerical dissipation being non-negative independently. The additional challenge is that this total numerical dissipation is to be controllable by the appropriate algorithmic parameters (so $\mathcal{D} = 0$ is an

option, recovering the original conserving scheme) and leads to, at least, second order accurate approximations in time. We note in this respect that the conserving approximation (3.29) and (3.30) are second order accurate. To address this challenge, we follow similar arguments as proposed in Armero and Romero (2001a, b) in the simpler context of nonlinear continuum elastodynamics, arriving to first and second order accurate energy-dissipative momentum-conserving schemes or, in short, EDMC-1 and EDMC-2 schemes, respectively.

Remark 3.2. The above considerations use explicitly the elastic tangent matrices (2.14). The general case can be easily accommodated with a fixed tangent $\partial^2 W$ or its convexification to recover a positive definite tangent. Note that all the developments apply to a given time step $[t_n, t_{n+1}]$. We refer to Armero and Romero (2001a, b) for a detailed discussion of these issues in the context of nonlinear continuum elastodynamics.

3.4.1 A first order dissipative scheme

A first order scheme, called EDMC-1, is easily obtained with the quadratic expressions

$$\mathcal{D}_\Gamma = \tfrac{1}{2}\chi_\Gamma \|\boldsymbol{\Gamma}^h_{n+1} - \boldsymbol{\Gamma}^h_n\|^2_{\mathbb{C}_\Gamma} \quad \text{and}$$
$$\mathcal{D}_\Omega = \tfrac{1}{2}\chi_\Omega \|\boldsymbol{\Omega}^h_{n+1} - \boldsymbol{\Omega}^h_n\|^2_{\mathbb{C}_\Omega} \ , \tag{3.42}$$

for the dissipation densities associated with the stress resultants, and

$$\mathcal{D}_v = \tfrac{1}{2}\chi_v A_{\rho_o}(v_{n+1} - v_n)^2 \quad \text{and}$$
$$\mathcal{D}_v = \tfrac{1}{2}\chi_v A_{\rho_o}(v_{n+1} - v_n)^2 \ . \tag{3.43}$$

The definitions (3.42) and (3.43) introduce general (user-controlled) algorithmic parameters $\chi \geq 0$ that control the amount of numerical dissipation. We refer in particular to Armero and Romero (2001a) for a spectral analysis of the scheme in the context of a linear problem, showing the dependence of the numerical dissipation on the corresponding algorithmic parameter. The conserving case is easily recovered with the choice $\chi's = 0$.

We observe that, in this case, all four dissipation functions are non-negative for all $\chi's \geq 0$ and have the proper limits (3.35) and (3.40). The first order accuracy of the final scheme is clear. In particular, the dissipative parts of the stress resultants approximations reduce in this case to

$$\mathbf{N}_{\text{diss}} = \tfrac{1}{2}\chi_\Gamma \mathbb{C}_\Gamma(\boldsymbol{\Gamma}_{n+1} - \boldsymbol{\Gamma}_n) \ , \quad \text{and}$$
$$\mathbf{M}_{\text{diss}} = \tfrac{1}{2}\chi_\Omega \mathbb{C}_\Omega(\boldsymbol{\Omega}_{n+1} - \boldsymbol{\Omega}_n) \ , \tag{3.44}$$

after using the general formulae (3.31) and (3.32).

3.4.2 A second order dissipative scheme

A second order dissipative scheme, referred to as EDMC-2, is obtained with the dissipation functions

$$\mathcal{D}_\Gamma = \tfrac{1}{2}\tilde{\beta}_\Gamma \|\boldsymbol{\Gamma}^h_{n+1} - \boldsymbol{\Gamma}^h_n\|^2_{\mathbb{C}_\Gamma} \quad \text{and}$$
$$\mathcal{D}_\Omega = \tfrac{1}{2}\tilde{\beta}_\Omega \|\boldsymbol{\Omega}^h_{n+1} - \boldsymbol{\Omega}^h_n\|^2_{\mathbb{C}_\Omega} \ , \tag{3.45}$$

in terms of the to-be-defined scalar parameters $\tilde{\beta}_\Gamma$ and $\tilde{\beta}_\Omega$, leading by (3.31) and (3.32) to the dissipative stress contributions

$$\mathbf{N}_{\text{diss}} = \tfrac{1}{2}\tilde{\beta}_\Gamma \mathbb{C}_\Gamma(\boldsymbol{\Gamma}^h_{n+1} - \boldsymbol{\Gamma}^h_n), \quad \text{and}$$
$$\mathbf{M}_{\text{diss}} = \tfrac{1}{2}\tilde{\beta}_\Omega \mathbb{C}_\Omega(\boldsymbol{\Omega}^h_{n+1} - \boldsymbol{\Omega}^h_n) \ , \tag{3.46}$$

and the velocity dissipation functions

$$\mathcal{D}_v = \tfrac{1}{2}A_{\rho_o}(\tilde{v}_n - v_n)(v_{n+1} - v_n), \quad \text{and}$$
$$\mathcal{D}_v = \tfrac{1}{2}A_{\rho_o}(\tilde{v}_n - v_n)(v_{n+1} - v_n) \ , \tag{3.47}$$

in terms of the scalar parameters $\tilde{v}_n$ and $\tilde{v}_n$. Motivated by the L-stable second-order Runge–Kutta family of one-step schemes identified in Armero and Romero (2001b), these parameters are defined implicitly by the linear set of algebraic equations

$$\left.\begin{aligned}
\tilde{\beta}_\Gamma &= \alpha_{\Gamma v}\frac{\Delta t}{h}(\tilde{v}_n - v_{n+1}) + \alpha_{\Gamma v}\frac{\Delta t}{h}(\tilde{v}_n - v_{n+1}),\\
\tilde{\beta}_\Omega &= \alpha_{\Omega v}\frac{\Delta t}{h}(\tilde{v}_n - v_{n+1}) + \alpha_{\Omega v}\frac{\Delta t}{h}(\tilde{v}_n - v_{n+1}),\\
\tilde{v}_n &= v_n - \frac{\Delta t}{A_{\rho_o} h}\Big[\alpha_{\Gamma v}(\tilde{\beta}_\Gamma - 1)\|\boldsymbol{\Gamma}^h_{n+1} - \boldsymbol{\Gamma}^h_n\|^2_{\mathbb{C}_\Gamma}\\
&\qquad + \alpha_{\Omega v}(\tilde{\beta}_\Omega - 1)\|\boldsymbol{\Omega}^h_{n+1} - \boldsymbol{\Omega}^h_n\|^2_{\mathbb{C}_\Omega}\Big],\\
\tilde{v}_n &= v_n - \frac{\Delta t}{A_{\rho_o} h}\Big[\alpha_{\Gamma v}(\tilde{\beta}_\Gamma - 1)\|\boldsymbol{\Gamma}^h_{n+1} - \boldsymbol{\Gamma}^h_n\|^2_{\mathbb{C}_\Gamma}\\
&\qquad + \alpha_{\Omega v}(\tilde{\beta}_\Omega - 1)\|\boldsymbol{\Omega}^h_{n+1} - \boldsymbol{\Omega}^h_n\|^2_{\mathbb{C}_\Omega}\Big] \ ,
\end{aligned}\right\} \tag{3.48}$$

where h is a characteristic length, chosen to be the length associated with the quadrature point at which the equations above are enforced (e.g. $h = w_l j_l$ for the quadrature weight w_l and the Jacobian j_l of the isoparametric map for the finite element in the interpolation of the undeformed middle-axis of the rod). As noted above, all the formulae (3.48) are to be evaluated at the quadrature points for the dissipative parts of the stress resultants and velocities. The presence of a length parameter is required for the proper dimensional consistency of the final equations. Furthermore, a calculation shows that the equations are well-defined in the limit $h \to 0$, after noting that the stress resultants are eventually multiplied by the length parameter again h in the numerical implementation. In fact, a vanishing dissipation is obtained in this limit, as it should be expected. The scalars $\alpha's$ are general user-controlled algorithmic parameters that control the amount of numerical dissipation introduced by the numerical scheme.

An algebraic calculation using the definitions (3.48) shows that the final expression of the numerical dissipation (3.41) reads in this case

$$\mathcal{D} = \int_0^L [\mathcal{D}_v + \mathcal{D}_v + \mathcal{D}_\Gamma + \mathcal{D}_\Omega]\, \mathrm{d}S$$

$$= \int_0^L \left[\frac{1}{2} A_{\rho_o} (\tilde{v}_n - v_n)^2 + \frac{1}{2} A_{\rho_o} (\tilde{v}_n - v_n)^2 + \frac{1}{2} \tilde{\beta}_\Gamma^2 \| \mathbf{\Gamma}_{n+1} - \mathbf{\Gamma}_n \|^2_{\mathbb{C}_\Gamma} + \frac{1}{2} \tilde{\beta}_\Omega^2 \| \mathbf{\Omega}_{n+1} - \mathbf{\Omega}_n \|^2_{\mathbb{C}_\Omega} \right] \mathrm{d}S \geq 0 \ , \qquad (3.49)$$

after a cancellation of the terms involving the same algorithmic parameter α in the cross definitions (3.48) of the parameters associated to the stress resultants and the velocity approximations. We observe that, in this case, the individual dissipation functions (3.46) and (3.47) are not necessarily positive, but their sum in (3.49) is indeed nonnegative thanks to the definition of these cross terms. We can observe also that the choice $\alpha's = 0$ for all the algorithmic parameters recovers again the energy conserving scheme (i.e. $\mathbf{N}_{\text{diss}} = 0$, $\mathbf{M}_{\text{diss}} = 0$, $\mathbf{v}_{\text{diss}} = 0$ and $\mathbf{v}_{1,\text{diss}} = \mathbf{v}_{2,\text{diss}} = 0$). We refer again to Armero and Romero (2001b) for a complete spectral analysis of the scheme in the context of a linear problem showing the dependence of the numerical dissipation on the algorithmic parameters. In particular, this analysis confirms the introduction of this numerical dissipation in the high-frequency range, with the final scheme being second-order accurate in time.

Remarks 3.3. 1. We note that the numerical simulations presented in Sect. 5 consider a reduced quadrature in the evaluation of the stress terms of the governing equations (3.6) to avoid the well-known shear locking in beam formulations. On the other hand, the inertial terms are integrated with a full quadrature rule. The nonnegative character of the numerical dissipation depends on the cancellation of terms pointed out above to arrive at the final expression (3.48) under the integral sign. Observe that the parameters $\tilde{\beta}'s$ and $\tilde{v}'s$ affect the dissipative approximations of the stress resultants and the velocities. In the numerical setting, this cancellation must occur at the quadrature points, with the different terms requiring their evaluation at the same points. This is accomplished by the evaluation of all the integrals involving the dissipative part of the approximation of the generalized velocities with the same reduced quadrature rule as the stress resultant terms. For example, the translational part of Eq. (3.7) has to be understood as

$$\underbrace{\int_0^L \frac{\mathbf{r}^h_{n+1} - \mathbf{r}^h_n}{\Delta t} \cdot \delta \mathbf{v}^h \, \mathrm{d}S}_{\text{full quadrature}} - \left[\underbrace{\int_0^L \mathbf{v}_{\text{cons}} \cdot \delta \mathbf{v}^h \, \mathrm{d}S}_{\text{full quadrature}} + \underbrace{\int_0^L \mathbf{v}_{\text{diss}} \cdot \delta \mathbf{v}^h \, \mathrm{d}S}_{\text{reduced quadrature}} \right] = 0 \ , \qquad (3.50)$$

for all $\delta \mathbf{v}^h \in T\mathcal{W}^h$. A similar evaluation must be employed for the director velocity equations. The numerical simulations presented in Sect. 5 consider a linear finite elements with the two-point Gauss quadrature rule for the transient terms and the reduced one-point quadrature rule for the stress resultant terms.

2. It is important to observe that the formulae (3.48) defining the dissipative approximations involve only the values of the configuration variables and their velocities at t_n and t_{n+1}, that is, $(\mathbf{\Phi}_n, \mathbf{W}_n)$ and $(\mathbf{\Phi}_{n+1}, \mathbf{W}_{n+1})$ in the compact notation introduced in previous sections. That is, the final scheme is a one-step method with no intermediate stages, as favored in the discussion of Sect. 1. The local equations (3.48) define simply a linear set of algebraic equations to be solved at each quadrature point for the scalar values $\tilde{\beta}_\Gamma$, $\tilde{\beta}_\Omega$, $\tilde{v}_n$ and $\tilde{v}_n$. These equations, however, fully couple the equations (3.6) and (3.7) in the configuration and the velocity variables. Their efficient solution can still be obtained through the numerical implementation described in the following section.

3. The final numerical schemes can be shown to satisfy the second part of Item **5.** in the list of requirements identified in the introductory discussion of Sect. 1, that is, the relative equilibria of the physical system are preserved exactly with the group motions associated to these solutions being approximated in a conservative matter. The numerical dissipation is then introduced in the internal modes of the motion. We refer Armero and Romero (2001a) for a complete discussion of these aspects in the context of nonlinear elastodynamics. Similar arguments and proofs apply to the case of interest herein. We only observe that the dissipative parts of the stress resultants and the velocities vanish for the case when the strain measures remain constant in a time step and the velocity norms remain constant in a time step, that is, for solutions corresponding to a relative equilibria consisting of a rigid body motions superposed to a fixed deformed configuration. Further details are omitted here.

4
The numerical implementation

We discuss in this section the numerical implementation of the method presented in the previous section. A standard finite element implementation could be followed in which the nonlinear algebraic equations resulting from the variational equations (3.6) and (3.7) are solved iteratively. This approach is computationally costly because, as noted in Remark 3.3.2, the equilibrium equation (3.6) and the velocity equation (3.7) are coupled for the EDMC-2 scheme through the cross terms of the dissipative stresses and velocities in (3.48). Consequently, twelve degrees of freedom (three displacements, three rotation increments and their corresponding velocities) must be used during this solution procedure for every node in the model. This situation is to be contrasted with the implementation of classical time-stepping algorithms, which reduce to the solution of a system of equations in the configuration variables (i.e., three displacements and three rotation increments in the case of interest), followed by nodal updates to recover the corresponding velocities.

To avoid this added computational cost and the complexity of the described implementation, we consider an iterative scheme that avoids these shortcomings. This solution strategy is based on the repeated solution of a system of equations in which the dissipative terms are held constant and thus, do not modify the standard linearization process. We refer to Armero and Romero (2001b) for a similar iterative scheme in the context of nonlinear continuum elastodynamics.

In what follows, we consider the particular case where the dissipative terms are introduced only on the translational degrees of freedom (i.e., terms involving the stress resultant $\mathbf{N}$ and the velocity $\mathbf{v}$), as considered in the numerical simulations presented in Sect. 5. This choice amounts to the selection $\chi_\Omega = \chi_v = 0$ in the EDMC-1 scheme and $\alpha_{\Gamma v} = \alpha_{\Omega v} = \alpha_{\Omega v} = 0$ in the EDMC-2 scheme. The flexibility of the general formulation presented in the previous section is then used to our advantage since this choice simplifies significantly the final numerical implementation while introducing the desired numerical dissipation in a very efficient manner. As noted in Sect. 5, the difficulties observed by the conserving (non-dissipative) schemes can be directly linked to the high-frequency response associated to the axial and transverse shear deformation modes of the rod. These choices of algorithmic parameters introduce precisely the numerical dissipation through these components of the rod's response. The implementation of the general case follows similar, but more complex, arguments; we refer to Remark 4.1.3 below for further details.

4.1
The finite element equations

The dynamic equilibrium equation (3.6) reads in residual form

$$\mathbf{r}^A := \mathbf{F}^A_{\text{ext}} - \mathbf{F}^A_{\text{int}} - \mathbf{F}^A_{\text{iner}} = \mathbf{0} \ , \tag{4.1}$$

for $A = 1, 2, \ldots, n_{\text{node}}$. The three vectors $\mathbf{F}^A_{\text{ext}}, \mathbf{F}^A_{\text{int}}$ and $\mathbf{F}^A_{\text{iner}}$ correspond to the external, internal and inertial contributions, respectively. They are defined as

$$\mathbf{F}^A_{\text{ext}} = \boldsymbol{\Xi}^{A,\text{T}}_{n+1/2} \int_0^L N^A \begin{Bmatrix} \bar{\mathbf{n}} \\ \bar{\mathbf{m}}^1 \\ \bar{\mathbf{m}}^2 \\ \mathbf{0} \end{Bmatrix} \mathrm{d}S \ , \tag{4.2}$$

$$\mathbf{F}^A_{\text{int}} = \boldsymbol{\Xi}^{A,\text{T}}_{n+1/2} \int_0^L \mathbb{B}^{A,\text{T}}_{n+1/2} \begin{Bmatrix} \mathbf{N}^* \\ \mathbf{M}^* \end{Bmatrix} \mathrm{d}S \ , \tag{4.3}$$

$$\mathbf{F}^A_{\text{iner}} = \boldsymbol{\Xi}^{A,\text{T}}_{n+1/2} \int_0^L \frac{N^A}{\Delta t} \begin{Bmatrix} A_{\rho_o}(\mathbf{v}^h_{n+1} - \mathbf{v}^h_n) \\ \mathcal{I}^{1\beta}_{\rho_o}(\mathbf{v}^h_{\beta,n+1} - \mathbf{v}^h_{\beta,n}) \\ \mathcal{I}^{2\beta}_{\rho_o}(\mathbf{v}^h_{\beta,n+1} - \mathbf{v}^h_{\beta,n}) \\ \mathbf{0} \end{Bmatrix} \mathrm{d}S \ , \tag{4.4}$$

for $A = 1, 2, \ldots, n_{\text{node}}$, where the external and internal terms are evaluated using a reduced quadrature, with a full quadrature for the inertial terms.

The translational part of the velocity update equation (3.7) results in the equation

$$\int_0^L N^A A_{\rho_o} \frac{\mathbf{r}^h_{n+1} - \mathbf{r}^h_n}{\Delta t} \, \mathrm{d}S = \int_0^L N^A A_{\rho_o} \mathbf{v}^h_{n+1/2} \, \mathrm{d}S + \int_0^L N^A A_{\rho_o} \mathbf{v}_{\text{diss}} \, \mathrm{d}S \ , \tag{4.5}$$

where, according to Remark 3.3.1, the last integral is evaluated with a reduced quadrature rule. The first term in (4.5) defines the consistent mass matrix with components

$$\mathbf{M}^{AB} = \int_0^L N^A N^B A_{\rho_o} \, \mathrm{d}S \ . \tag{4.6}$$

Equation (4.5) reads then in matrix form

$$\sum_{B=1}^{n_{\text{node}}} \mathbf{M}^{AB} \frac{\mathbf{r}^B_{n+1} - \mathbf{r}^B_n}{\Delta t} = \sum_{B=1}^{n_{\text{node}}} \mathbf{M}^{AB} \mathbf{v}^B_{n+1/2} + \sum_{B=1}^{n_{\text{node}}} \mathbf{M}^{AB} \mathbf{g}^B \ , \tag{4.7}$$

where the vector $\mathbf{g}^B$ is obtained as the solution of the system

$$\mathbf{M}\mathbf{g}^A = \int_0^L N^A A_{\rho_o} \mathbf{v}_{\text{diss}} \, \mathrm{d}S \ , \tag{4.8}$$

for $A = 1, \ldots, n_{\text{node}}$. Equation (4.7) reduces then to the nodal update equation

$$\frac{1}{\Delta t}(\mathbf{r}^A_{n+1} - \mathbf{r}^A_n) = \mathbf{v}^A_{n+1/2} + \mathbf{g}^A \ , \tag{4.9}$$

for $A = 1, \ldots, n_{\text{node}}$. When compared with the implementation of a standard mid-point or energy–conserving solution of the problem, we observe that the difference in these equations stems only from the last term $\mathbf{g}^A$ in (4.9). We observe that the computation of the vector $\mathbf{g}^A$ requires the solution of the system (4.8), but involving the fixed (symmetric positive definite) mass matrix (4.6). Hence, a single Cholesky decomposition is required in a simulation, with the computation of the vector $\mathbf{g}^A$ involving only a forward and a backward substitution.

As noted above, we consider the case with a conserving approximation for the rotational degrees of freedom. Let

$$\mathbf{d}^A_{i,n+1} = \exp[\hat{\boldsymbol{\theta}}^A]\mathbf{d}^A_{i,n} \ , \quad i = 1, 2, 3 \ , \tag{4.10}$$

for $A = 1, \ldots, n_{\text{node}}$ (no summation implied in the repeated nodal indices A in this and later expressions, unless an explicit summation symbol is present). The vector $\boldsymbol{\theta}^A$ is the incremental rotation vector of the nodal frame $\{\mathbf{d}_1, \mathbf{d}_2, \mathbf{d}_3\}$ and $\exp[\hat{\boldsymbol{\theta}}]$ is the exponential map of the associated skew symmetric tensor. This update enforces nodally the orthogonality of the directors. Next define the pseudo rotation vector by the relation

$$\text{cay}[\bar{\boldsymbol{\theta}}^A] = \exp[\hat{\boldsymbol{\theta}}^A] \ , \tag{4.11}$$

where $\text{cay}[\cdot] : \mathbb{R}^3 \to SO(3)$ is the Cayley transform defined as

$$\text{cay}[\mathbf{a}] = \left(\mathbf{1} + \tfrac{1}{2}\hat{\mathbf{a}}\right)\left(\mathbf{1} - \tfrac{1}{2}\hat{\mathbf{a}}\right)^{-1} \ . \tag{4.12}$$

This last definition can be used to rewrite the update (4.10) in the more convenient form

$$\begin{aligned} &\mathbf{d}^A_{i,n+1} = \text{cay}[\bar{\boldsymbol{\theta}}^A]\mathbf{d}^A_{i,n} \\ &\Rightarrow\ \mathbf{d}^A_{i,n+1} - \mathbf{d}^A_{i,n} = \bar{\boldsymbol{\theta}}^A \times \mathbf{d}^A_{i,n+1/2} \ , \end{aligned} \tag{4.13}$$

at each node $A = 1, n_{\text{node}}$.

However, two adjacent elements which connect at a node but are not aligned may have different section directors at the connecting node. Therefore, the update (4.13) must be modified accordingly. To this purpose, let $e = 1, \ldots, n_{\text{elem}}$ be the element number and denote by $\mathbf{d}_i^{(e)l}, v_i^{(e)l}$ the director and director velocity at the local node l of element e. The global-to-local nodal numbering map is given in terms of a Boolean matrix, often denoted by ID. Using this common naming convention, the global number of a node with local number l in an element e is $A = \text{ID}(e, l)$. The following modification of (4.13) is considered, which accounts for different section directors in connecting elements

$$\begin{aligned} &\mathbf{d}^{(e),l}_{i,n+1} = \text{cay}[\bar{\boldsymbol{\theta}}^A]\mathbf{d}^{(e),l}_{i,n}, \quad i = \{1,2,3\} \quad \text{with} \\ &A = \text{ID}(e,l) \ . \end{aligned} \tag{4.14}$$

Finally, the director velocities are approximated by the following mid-point rule at the element level

$$\begin{aligned} &\mathbf{v}^{(e)l}_{i,n+1} = -\mathbf{v}^{(e)l}_{i,n} + 2\tilde{\boldsymbol{\omega}}^A \times \mathbf{d}^{(e)l}_{i,n+1/2} \ , \quad \text{with} \\ &A = \text{ID}(e,l) \ . \end{aligned} \tag{4.15}$$

for $i = \{1,2,3\}$ and the nodal angular velocity $\tilde{\boldsymbol{\omega}}^A = \bar{\boldsymbol{\theta}}^A/\Delta t$.

4.2
Summary of the numerical implementation

In summary, the numerical solution of the fully discrete equations of motion involves the solution of the residual equation (4.1) together with the nodal updates (4.9) and (4.15). The difference with a conserving scheme is the last term in (4.9). An iterative strategy is proposed next that takes advantage of the similarities of the conserving and dissipative formulations.

In this way, a number of iterations `NITER` is chosen and the following steps are executed:

0. Calculate the mass matrix (4.6) and its Cholesky decomposition.

1. Given the nodal variables $(\boldsymbol{\Phi}^A_n, \mathbf{W}^A_n)$, with $A = 1, \ldots, n_{\text{node}}$, at time t_n,

2. obtain a predictor for the solution at t_{n+1}

$$(\boldsymbol{\Phi}^{A,(o)}_{n+1}, \mathbf{W}^{A,(o)}_{n+1}) = (\boldsymbol{\Phi}^A_n, \mathbf{W}^A_n) \ , \tag{4.16}$$

and set the counter `ITER=0`.

3. Evaluate the dissipative terms $\mathbf{N}_{\text{diss}}$ and $\mathbf{v}_{\text{diss}}$ corresponding to the EDMC formulae as functions of the solution at time t_n and the current iterate $(\boldsymbol{\Phi}^A_{n+1}, \mathbf{W}^A_{n+1})$. Calculate the vector $\mathbf{g}$ solving (4.8) through the already available (fixed) Cholesky decomposition of the mass matrix. Increment the counter `ITER` by 1.

4. Solve the nonlinear finite element equations (4.1) holding constant the dissipative terms $\mathbf{N}_{\text{diss}}$ and $\mathbf{v}_{\text{diss}}$. An iterative Newton–Raphson procedure can be used to this purpose; see Remark 4.1.1 below. Denoting by k the iteration count this solution procedure accounts for:

4.1. Solve the linearized residual equations for the increments $\Delta\boldsymbol{\Phi}^A = (\Delta\mathbf{r}^A, \Delta\bar{\boldsymbol{\theta}}^A)$ making use of the linear velocity updates (4.9) and (4.15).

4.2. Update the configuration variables

$$\mathbf{r}^{A,(k+1)}_{n+1} = \mathbf{r}^{A,(k)}_{n+1} + \Delta\mathbf{r}^A \ , \tag{4.17}$$

$$\boldsymbol{\Lambda}^{A,(k+1)}_{n+1} = \text{cay}[\Delta\bar{\boldsymbol{\theta}}^A]\boldsymbol{\Lambda}^{A,(k)}_{n+1} \ , \tag{4.18}$$

4.3. Update the nodal velocity variables. For every node $A = 1, \ldots, n_{\text{node}}$

$$\mathbf{v}^{A,(k+1)}_{n+1} = \mathbf{v}^{A,(k)}_{n+1} + \frac{2}{\Delta t}\Delta\mathbf{r}^A \ , \tag{4.19}$$

$$\bar{\boldsymbol{\theta}}^A = \text{cay}^{-1}[\boldsymbol{\Lambda}^{A,(k+1),T}_{n+1}\boldsymbol{\Lambda}^A_n] \ , \tag{4.20}$$

$$\tilde{\boldsymbol{\omega}}^{A,(k+1)} = \frac{2}{\Delta t}\bar{\boldsymbol{\theta}}^A \ , \tag{4.21}$$

4.4. Update the director and the director velocities at the element (e) for every node in the element

$$\boldsymbol{\Lambda}^{(e),l,(k+1)}_{n+1} = \boldsymbol{\Lambda}^{A,(k+1)}_{n+1}\boldsymbol{\Lambda}^{(e),l}_o \ , \tag{4.22}$$

$$\mathbf{v}^{(e),l,(k+1)}_{i,n+1} = -\mathbf{v}^{(e)l}_{i,n} + 2\tilde{\boldsymbol{\omega}}^{A,(k+1)} \times \mathbf{d}^{(e),l,(k+1)}_{i,n+1/2} \ , \tag{4.23}$$

4.5. Check for convergence in the solution of the system of nonlinear equations and go back to **4.1** if not converged.

5. If the value of the counter `ITER` is less than `NITER`, go back to step **3.**

6. Advance the time step counter n and `GOTO` **1.**

Remarks 4.1. 1. Since the dissipative terms are held constant in the Newton–Raphson procedure of the solution step **4.1**, the consistent tangent matrix employed in this solution process is identical to the one associated to the fully conserving scheme, except for the definition of the stresses in the geometric tangent now accounting also for the constant dissipative part. A key factor for this aspect is the linearity of the velocity update equations which only holds true because the dissipative terms are kept constant in the Newton-Raphson loop. We refer to Romero and Armero (2002a) for complete details of the consistent linearization of the energy conserving scheme.

2. Different combinations of the constant `NITER` and the tolerance for the Newton–Raphson scheme can lead to different computational costs for the same solution. We refer to Armero and Romero (2001b) for a complete evaluation of this cost in the context of nonlinear continuum elastodynamics.

3. The general case involving dissipative terms in the rotational degrees of freedom follows similar arguments. The mass matrix associated to these degrees of freedom is not constant now, in contrast to (4.6) for the translational

degrees of freedom. This requires the solution of a system similar to (4.8) with a changing system matrix. This added cost motivates also the assumed choice of algorithmic parameters. Additional details are omitted.

5
Representative numerical simulations

We present in this section several numerical examples to illustrate the fundamental properties of the time-stepping algorithms formulated in this article. The first example illustrates the conservation laws of linear and angular momeda of the final discrete schemes while introducing a strictly non-negative numerical energy dissipation. The rest of examples illustrate how the added numerical dissipation enhances the stability of the time integration scheme, resulting in improved algorithms as compared with standard conserving methods.

5.1
Example 1: free flight of a three-dimensional frame

This first example consists of the free flight of a three-dimensional frame. This example was first considered in Romero and Armero (2002a) in the context of energy–momentum conserving schemes. The purpose here is to illustrate clearly the addition of non-negative energy dissipation, while preserving exactly the conservation of linear and angular momenta. The controllable character of this numerical dissipation is also illustrated with the recovery of the energy conserving scheme as a particular case.

The frame consists of three equal rods linked rigidly in two right angles as depicted in Fig. 2. The assumed material properties are: density $\rho_o = 500$, Young's modulus $E = 5 \cdot 10^5$ and Poisson ratio $\nu = 0.3$. The constant cross-section of the rod has area $A = 0.005$, a diagonal second moment of area with values $\tilde{I}^{11} = \tilde{I}^{22} = 2 \cdot 10^{-5}$ (that is, a circular cross–section with full symmetry) and torsional inertia $J = \tilde{I}^{11} + \tilde{I}^{22} = 4 \cdot 10^{-5}$. Each rod is modeled with five linear finite elements of equal length. As discussed in Remark 3.3.1, a reduced one-point quadrature rule is considered for the stress resultant terms to avoid shear locking.

The frame is set in motion by giving initial velocities to the connections A, B and C of Fig. 2 of values $\mathbf{v}_A = -\mathbf{e}_3$, $\mathbf{v}_B = 2\mathbf{e}_3$ and $\mathbf{v}_C = -\mathbf{e}_2$, respectively, in the frame also depicted in this figure. The frame is then in free flight afterwards. We consider the second-order energy-dissipating momentum-conserving scheme EDMC-2 developed in Sect. 3.4.2 with the choice of algorithmic parameters of Sect. 4 in terms of a single algorithmic parameter $\alpha \equiv \alpha_{\Gamma v}$. The values of $\alpha = 0$ and $\alpha = 0.5$ are considered for the algorithmic parameter in two different simulations. As noted in Sect. 3.4.2 the case $\alpha = 0$ recovers the energy–momentum scheme of Romero and Armero (2002a). Each simulation is performed with 50 time steps of equal size $\Delta t = 0.2$ for a total time of 10.

Figure 3 depicts the solution obtained with the EDMC-2 $\alpha = 0.5$. The deformed configuration of the frame is depicted every ten time steps. We observe that the motion involves large deformations, with a large straining of the rods. The accurate treatment of the rigid connections by the implementation described in Sect. 4, with two different directors for each rod connecting at the corner, is to be noted.

Figure 4 depicts the evolution of the three components of the linear momentum and the three components of the angular momentum as well as the total energy in the system, showing also the kinetic and potential energies separately. The full conservation of the momenta in this system in free flight can be observed for both cases (that is, for $\alpha = 0$ and $\alpha = 0.5$), confirming Proposition 3.1. Similarly, the numerical energy dissipation introduced in the simulation with $\alpha = 0.5$ can also be observed. The monotonic character of the energy dissipation is to be emphasized again, confirming the results of Sect. 3.4.

It is important to observe that this dissipation of the energy is not to a zero value, but to the energy associated to the relative equilibria associated to the constant linear and angular momentum of the system, as the long-term solution (not shown) confirms. We also observe that this dissipation can be turn off at any time by the choice $\alpha = 0$,

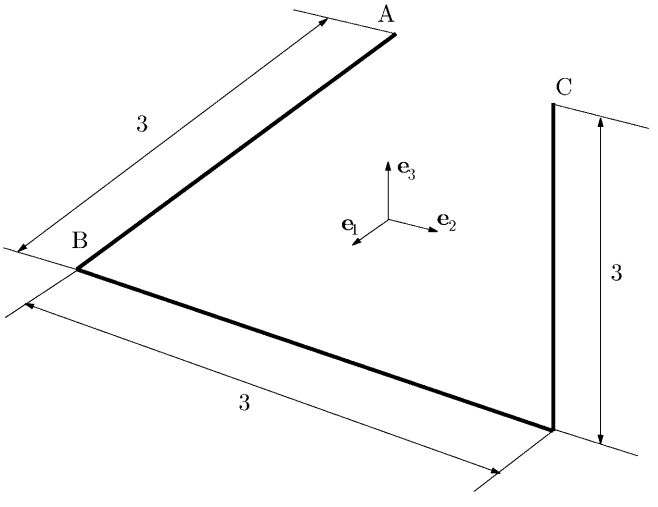

Fig. 2. Example 1: free flight of a three-dimensional frame. Geometry of the model: three rods modeled by five linear finite elements each are connected rigidly at the two junctions

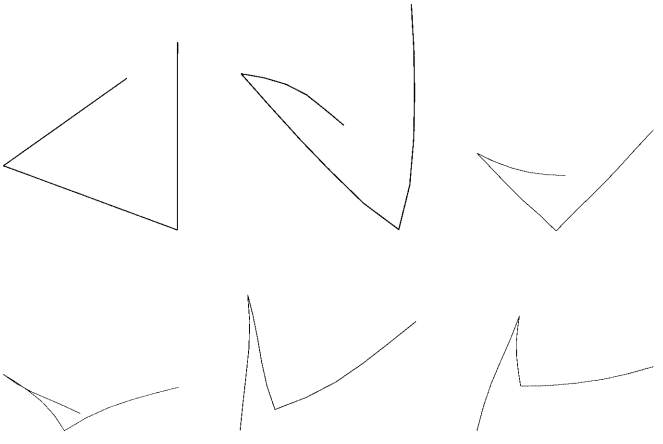

Fig. 3. Example 1: free flight of a three-dimensional frame. From left to right, top to bottom, deformed configurations every 10 time steps of size $\Delta t = 0.2$ in the EDMC-2 solution with $\alpha = 0.5$

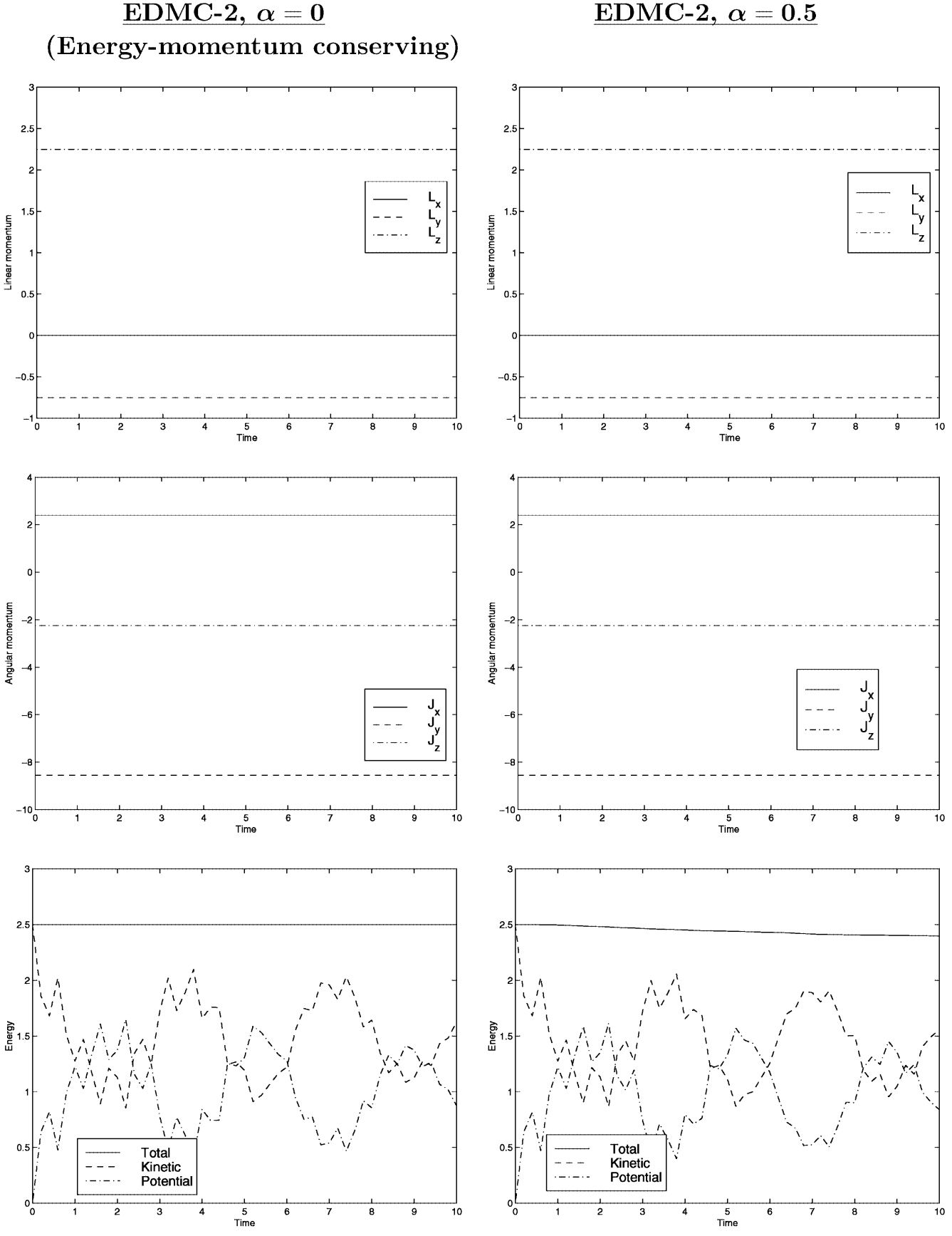

Fig. 4. Example 1: free flight of a three-dimensional frame. Linear and angular momentum and energy evolutions for the solutions obtained with the EDMC-2 scheme for $\alpha = 0$ (energy–momentum conserving) and $\alpha = 0.5$ (energy dissipative)

given the one-step nature of the scheme. The importance of considering this numerical dissipation to obtain the solution of the problem is illustrated in the next two examples.

5.2
Example 2: dynamic snap-through of a flexible arch

This second example considers the dynamic snap-through of a shallow arch. The geometry of the problem under consideration is depicted in Fig. 5. The arch is composed of two equal rods of cross-section areas $A = 0.1$, diagonal second moment of area $\tilde{I}^{11} = \tilde{I}^{22} = 5 \cdot 10^{-3}$, torsional constant $J = \tilde{I}^{11} + \tilde{I}^{22} = 10 \cdot 10^{-3}$, density $\rho_o = 5 \cdot 10^5$, Young's modulus $E = 2 \cdot 10^9$ and shear modulus $G = E/2$. The arch is modeled with a total of 30 identical linear rod elements.

A vertical force $\mathbf{F}$ is applied as depicted in Fig. 5 with modulus

$$\mathbf{F}(t) = \begin{cases} 2.5t, & 0 \le t \le 1000, \\ 0, & 1000 < t \ . \end{cases} \tag{5.1}$$

The motion occurs in the plane of the figure. After a certain level of the load, the arch snaps dynamically. This type of problems often exhibit a large amount of energy content in the high frequency range. Algorithms exhibiting a high-frequency dissipation are then crucial to obtain a stable numerical solution. We refer to Kuhl and Ramm (1996) for a similar problem and discussion in the context of nonlinear shells.

We consider again simulations with the energy–momentum conserving scheme (EDMC-2 scheme with $\alpha = 0$) and the EDMC-2 scheme with $\alpha \equiv \alpha_{\Gamma v} = 1$. A constant time step of $\Delta t = 1$ is considered for both cases. Figure 6 shows the evolution of the energy in each simulation, including again the evolutions of the potential and kinetic energies separately.

We observe that the energy conserving solution ($\alpha = 0$) fails to converge after the time $t = 1163$, long after the snap-through, which takes place at the time $t \approx 950$. Therefore, the reason for this lack of convergence cannot be that the size of the time step is too large to correctly capture the dynamics of the snap–through. A better explanation comes from the fact that the snap-through excites the high frequency modes of vibration of the structure. The evolutions of the kinetic and potential energies show the nature of the solution, involving fast oscillations. This result confirms the limitations of fully energy-conserving algorithms in these situations where the high numerical stiffness of the system may even preclude the convergence of the solution process of the nonlinear problem.

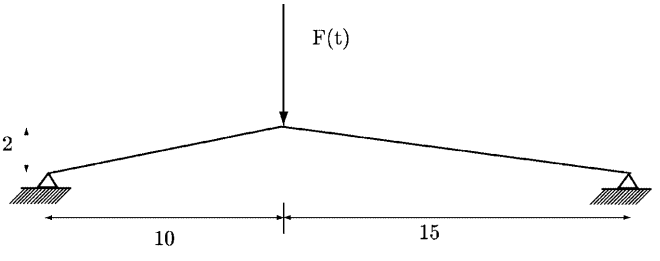

Fig. 5. Example 2: dynamic snap-through of flexible arch. Geometry of the problem

In contrast, the dissipative scheme shows no difficulties to converge with the considered time step. Figure 6 shows this solution up to the time $t = 2000$. The added dissipation in the axial modes of deformation through the non-zero algorithmic parameter $\alpha_{\Gamma v}$ allows the method to better control the overall solution. Note also in Fig. 6 that this is done while controlling the energy growth after the release of the external force. We investigate further these performances of the conserving and dissipative schemes with the size of the time step in the following example.

5.3
Example 3: dynamic simulation of a plane mechanism with rigid links

The use of time integration algorithms with high-frequency dissipation is specially useful in the simulation of multibody systems, involving mechanisms with links of different stiffnesses, all the way to the limit of rigid links. This type of problems are commonly associated to stiff differential equations. The stiffness of the equations results from the constraints in the limit case of rigid links and, in general, from the wide range of flexibilities in the bodies of these systems. Furthermore, sudden changes in the stiffness of the mechanisms in their deformed configurations, as for example occurs when the different links align, are responsible for the transfer of energy to the high frequency modes of the motion. This, in turn, causes problems to conserving schemes as identified in Bauchau et al. (1995).

Following these ideas, we proposed in Armero and Romero (2001a) a two dimensional mechanism composed of two rigid links and a flexible link, the latter modeled by springs and point masses. This simple setting allowed to study the effects described above. We consider again this mechanism but now with the flexible link modeled more realistically by an elastic Cosserat rod, as developed in this paper. The rigid links are modeled simply by a stiff axial element in conjunction with an augmented Lagrangian scheme to enforce the inextensibility constraint.

Figure 7 depicts the initial geometry of the mechanism. It is composed of two lateral rigid links of unit length connected by a flexible rod, also of unit length, all in a single plane. Each of the rigid links has one fixed end and one point mass of value $m = 2$ at the other end connecting with the flexible rod. The flexible link is modeled with 4 linear rod elements, of cross section $A = 0.08$, diagonal second moment of area $\tilde{I}^{11} = \tilde{I}^{22} = 10^{-4}$, torsional constant $J = \tilde{I}^{11} + \tilde{I}^{22}$, density $\rho = 10$, Young's modulus $E = 25 \cdot 10^3$ and Poisson ratio $v = 0.3$. A point load $\mathbf{F}$ of value

$$\mathbf{F}(t) = (-25\mathbf{e}_2 + 2\mathbf{e}_3) \cdot \begin{cases} 8t, & 0 \le t \le 0.25, \\ 4 - 8t, & 0.25 \le t \le 0.5, \\ 0, & 0.5 < t \ . \end{cases}$$

is applied on the mechanism at the point shown in Fig. 7. Due to the load $\mathbf{F}$, the mechanism swings in its plane, resulting in the repeated alignment of the rigid and flexible links. As discussed above, this situation generates a large

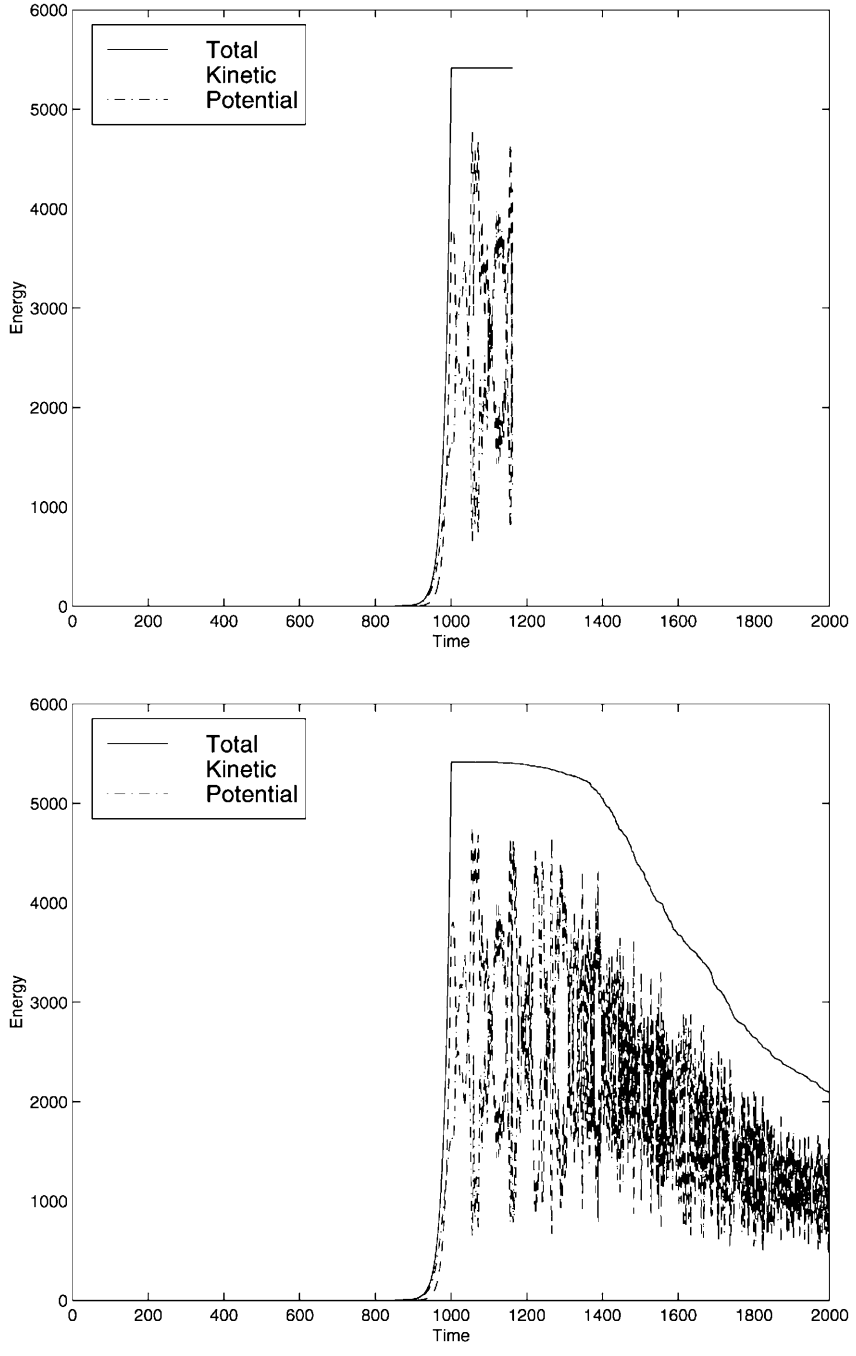

Fig. 6. Example 2: dynamic snap-through of plane arch. Energy evolution in the solutions obtained with the energy–momentum scheme (EDMC-2 with $\alpha = 0$) and the EDMC-2 with parameter $\alpha \equiv \alpha_{\Gamma v} = 1$. The time step size is $\Delta t = 1$ in both simulations

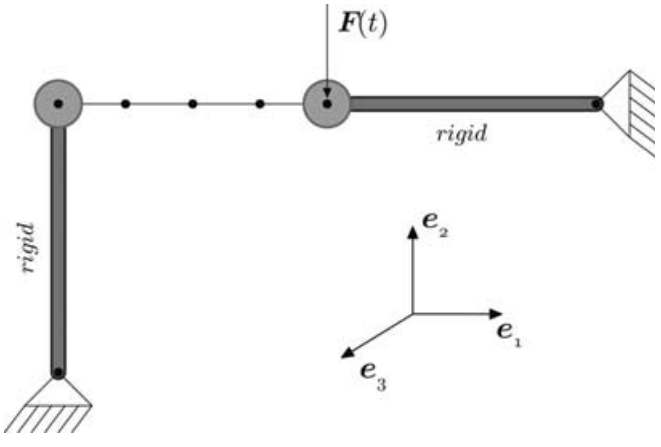

amount of energy content in the high-frequency part of the response. Figure 8 depicts the solution obtained with the EDMC-2 scheme with $\alpha = 0.5$, illustrating this motion.

We consider again simulations with the EDMC-2 dissipative scheme (with different algorithmic parameters $\alpha > 0$) and the energy–momentum conserving scheme (EDMC-2 with $\alpha = 0$), with now different values of the constant time-step sizes Δt. The solution obtained with the energy–momentum method fails to converge when the time step size is $\Delta t = 0.05$ and also when it is reduced to

◀

Fig. 7. Example 3: mechanism with constraints. Configuration at time $t = 0$

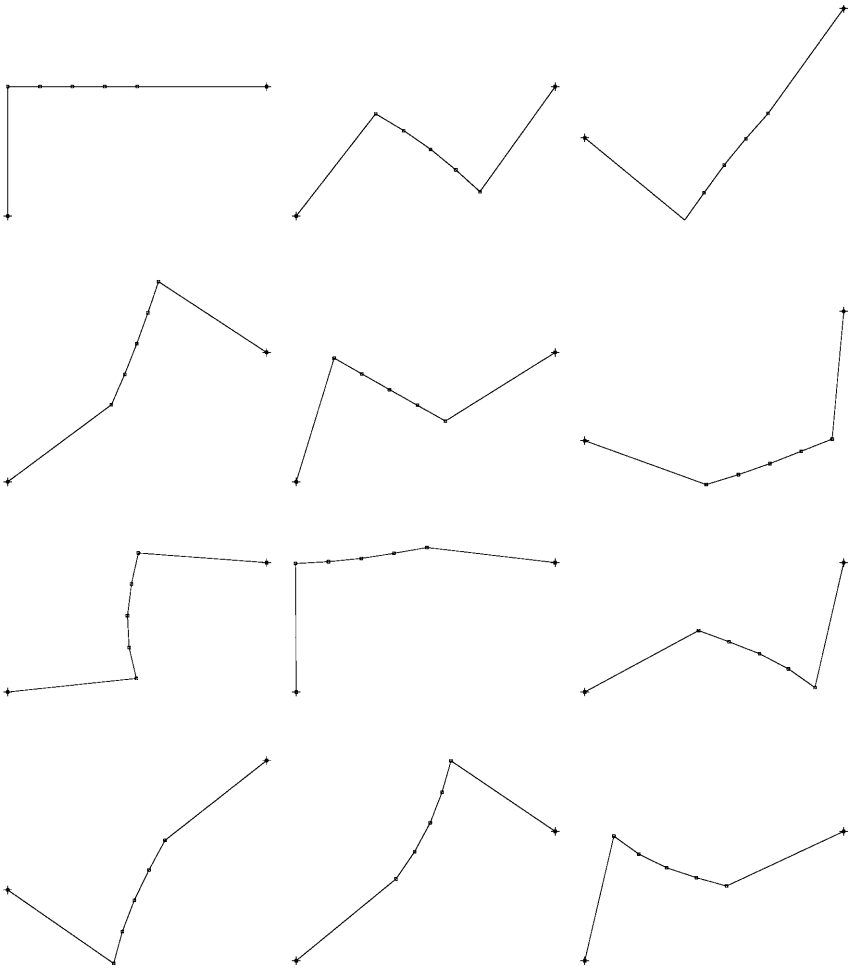

Fig. 8. Example 3: three link mechanism. From left to right, top to bottom, configurations of the mechanism at every 10 time steps of size $\Delta t = 0.05$ in the solution obtained with the EDMC-2 and $\alpha = 0.5$

$\Delta t = 0.01$ and 0.005. As pointed out in Bauchau et al. (1995), reducing the time step size in situations like the one under consideration does not help the numerical convergence, since new higher modes may enter in the solution as the time step size gets smaller making the convergence even harder. Figure 9 shows the deformed configuration of the mechanism in the last converged solution ($t \approx 3.3$) obtained with the energy–momentum method and $\Delta t = 0.05$. The alignment to follow of the rigid and flexible links of the mechanism can be observed in the figure. The limitations of the energy conserving scheme in handling these highly stiff systems in then confirmed.

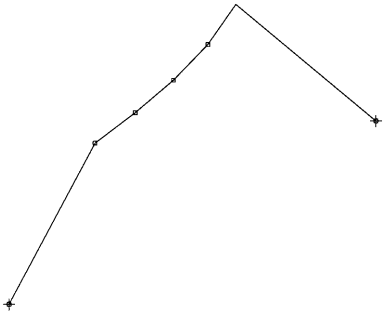

Fig. 9. Example 3: three link mechanism. Configuration of the mechanism in the last converged solution obtained with the energy–momentum scheme (EDMC-2 $\alpha = 0$) and $\Delta t = 0.05$

The solution computed with the EDMC-2 method converges for all these three time step sizes. When $\Delta t = 0.05$ the dissipation parameter is chosen to be $\alpha = 0.5$. For the other two cases, a value of $\alpha = 5.0$ is considered. Figure 8 shows the deformed configurations of the mechanisms computed with the time step size of $\Delta t = 0.05$ every ten time steps. Figure 10 shows the evolution of the energy in the three simulations, for the energy–momentum scheme and the EDMC-2 scheme. We depict again the total energy as well as its two components, the kinetic and potential energies. The high-frequency content of the solution becomes apparent before the energy–momentum fails to converge; see especially the plot for the time step $\Delta t = 0.005$. A good agreement can be observed before the failure of the energy–momentum scheme of this scheme with the dissipative EDMC-2 $\alpha > 0$ schemes. These plots illustrate clearly the effect of the numerical dissipation introduced by the latter. In particular, we observe that the energy is never allowed to grow

▶

Fig. 10. Example 3: three link mechanism. Evolution of the energies (total, kinetic and potential) in the solutions obtained with the energy–momentum (left column) and EDMC-2 $\alpha > 0$ (right column) for different time-step sizes. Observe the high–frequency energy of the solution right before the energy-conserving schemes fails to converge in contrast with the EDMC-2 scheme with $\alpha > 0$

EDMC-2, $\alpha = 0$
(Energy-momentum conserving)

EDMC-2, $\alpha > 0$

$\Delta t = 0.05$

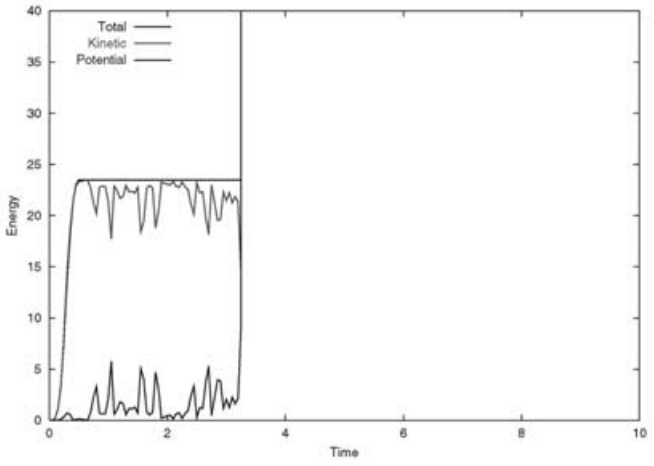

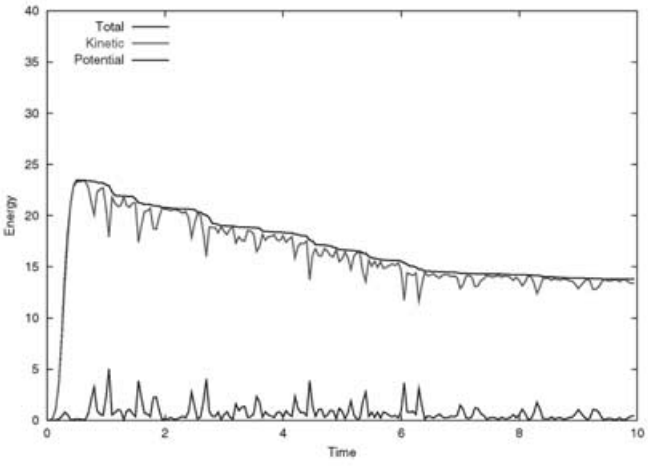

$\Delta t = 0.01$

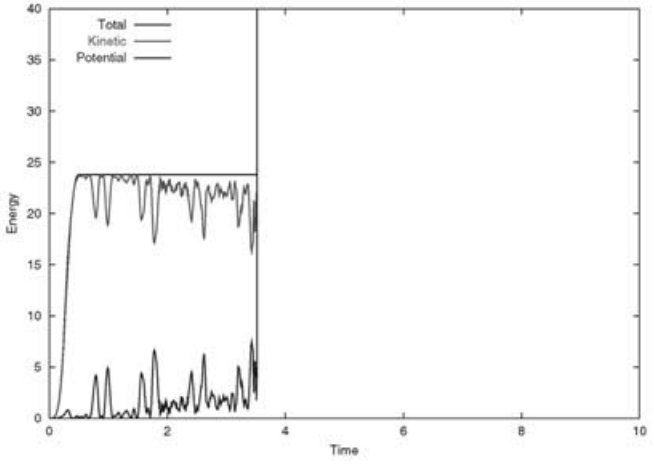

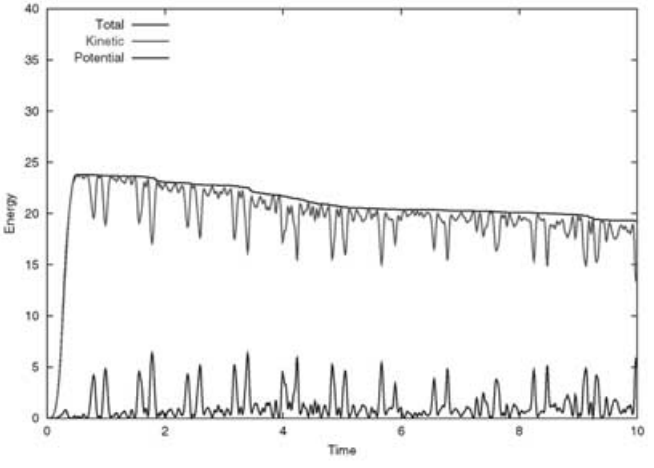

$\Delta t = 0.005$

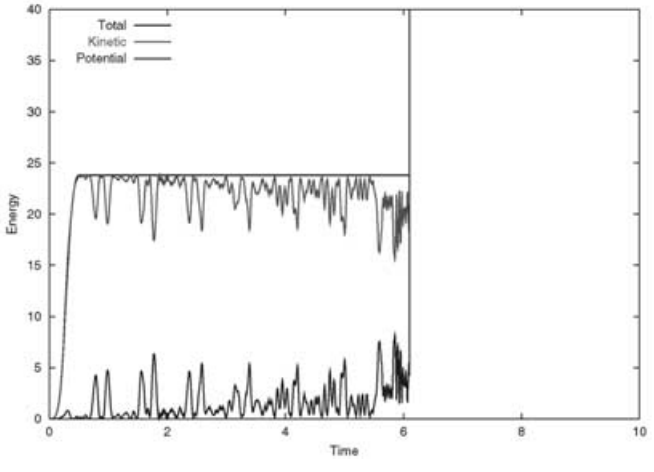

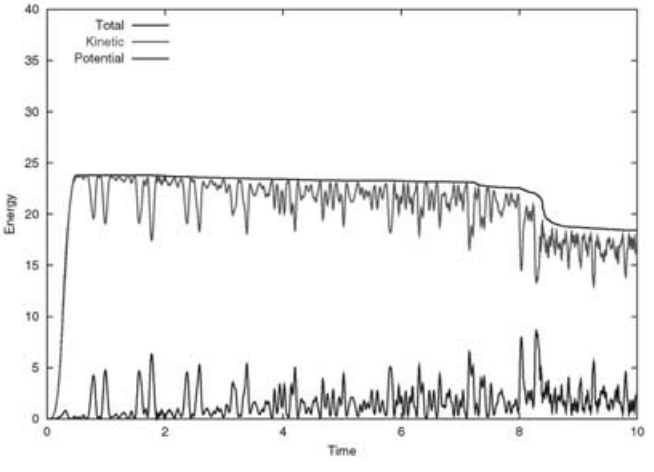

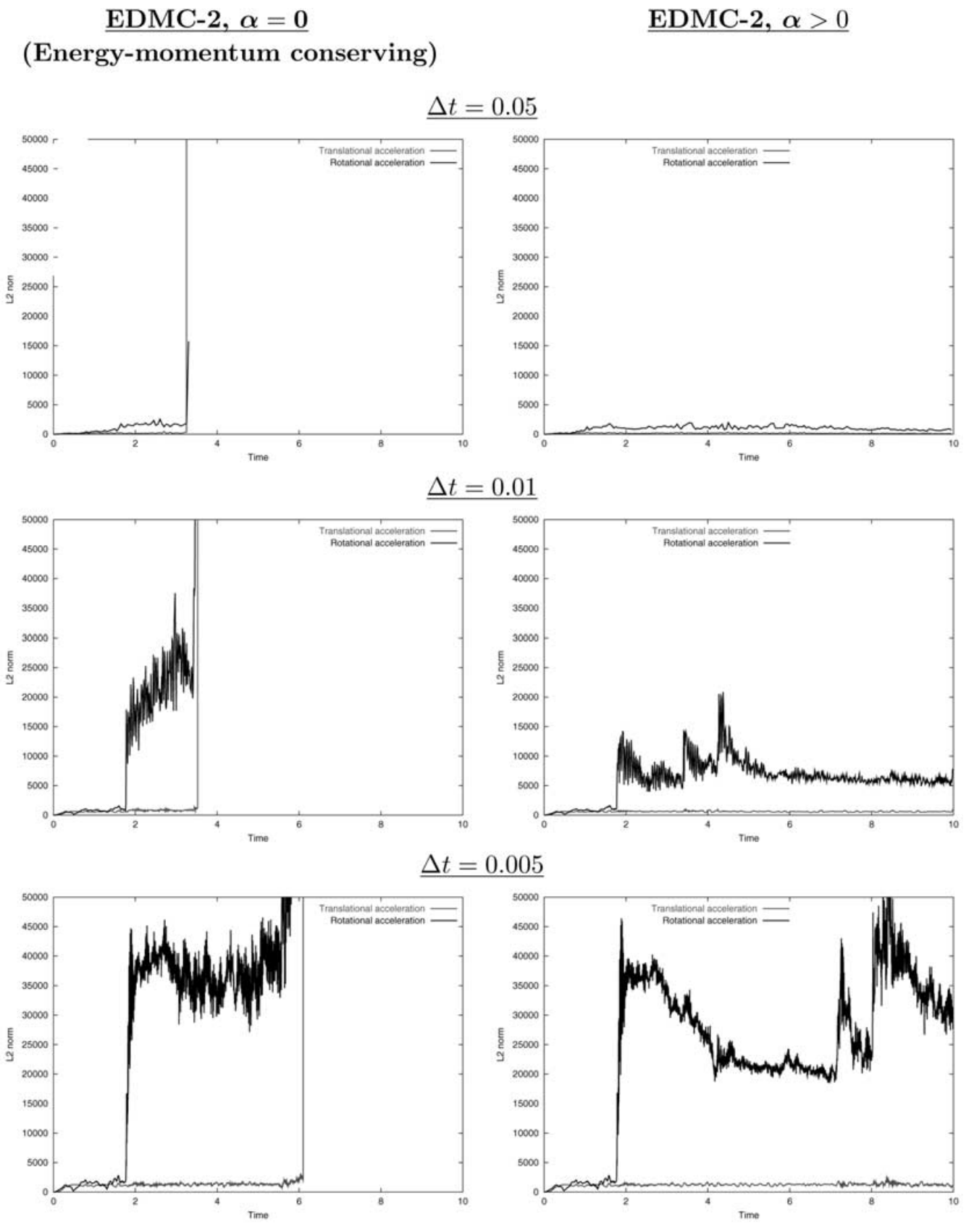

Fig. 11. Example 3: three link mechanism. Evolution of the acceleration norms in the solutions obtained with the energy–momentum (left column) and EDMC-2 $\alpha > 0$ (right column) for different time-step sizes. Observe the lack of control in the energy-conserving solution in contrast with the solutions obtained with the EDMC-2 scheme with $\alpha > 0$

after the initial loading phase in the EDMC-2 $\alpha > 0$. A smaller decrease of the energy can be observed the smaller the time step. We can also observe the localized effects of this numerical dissipation when the potential energy shows a spike and an increased oscillation in the high-frequency afterwards.

The evolution of the L_2 norm of the acceleration also provides important information about how the method controls the evolution of the high frequency content of the solution [see e.g. the discussion in Hughes (1987)]. Figure 11 shows the evolution of this norm for the translational and rotational accelerations in the solutions obtained with the energy–momentum and EDMC-2 methods. In the former case, the solutions exhibit an uncontrolled growth of the acceleration norms that can be associated to an instability in the numerical solution. We can observe how this growth leads eventually to a failure of the convergence in the solution of the nonlinear algebraic equations. In contrast, we can observe in the same Fig. 11 how the EDMC-2 algorithm controls the growth of these acceleration norms, avoiding altogether this instability, thanks to the added numerical dissipation. The robustness gained by the presence of the algorithmic parameters adding non-negative numerical dissipation to the solution process is then apparent.

6
Concluding remarks

We have discussed in this paper the formulation of energy–dissipative momentum conserving time stepping algorithms for the integration of the nonlinear dynamics of Cosserat rods. The newly proposed schemes exhibit these conservation/dissipation properties rigorously proven in the general nonlinear range, with the numerical dissipation introduced by the numerical scheme being controllable through the appropriate algorithmic parameters. An energy-conserving scheme is recovered as a particular case. We have discussed the details of the numerical implementation of the final schemes in the context of finite element interpolations of the governing equations that preserved the frame indifference of the strain and stress measured of the underlying physical system.

The final numerical schemes have shown to exhibit the necessary robustness to deal with the highly numerical stiff problems considered here. In particular, the added control on the evolution of the energy has shown to lead to improved, more stable, numerical simulations over the energy conserving schemes. We believe that this improved performance at a competitive computational cost makes these schemes an attractive alternative for this type of systems.

References

Antman SS (1992) Nonlinear problems of elasticity. Springer-Verlag

Armero F, Petocz E (1996) Formulation and analysis of conserving algorithms for frictionless dynamic contact/impact problems. Comput. Meth. Appl. Mech. Eng. 158: 269–300

Armero F, Romero I (2001a) On the formulation of high-frequency dissipative time-stepping algorithms for nonlinear dynamics. Part I: low order methods for two model problems and nonlinear elastodynamics. Comput. Meth. Appl. Mech. Eng. 190: 2603–2649

Armero F, Romero I (2001b) On the formulation of high-frequency dissipative time-stepping algorithms for nonlinear dynamics. Part II: high order methods. Comput. Meth. Appl. Mech. Eng. 190: 6783–6824.

Armero F, Romero I (2001c) On the objective and conserving integration of geometrically exact rod models. In: Wall WA, Bletzinger KU, Schweizerhof K (Eds) Trends in Computational Structural Mechanics. CIMNE, Barcelona, Spain.

Bauchau OA, Theron NJ (1996) Energy decaying scheme for non-linear beam models. Comput. Meth. Appl. Mech. Eng. 134: 37–56

Bauchau OA, Damilano G, Theron NJ (1995) Numerical integration of non-linear elastic multibody systems. Int. J. Numer. Meth. Eng. 38(16): 2727–2751

Betsch P, Steinmann P (2002) Frame-indifferent beam finite elements based upon the geometrically exact beam theory. Int. J. Numer. Meth. Eng. 54: 1775–1788

Botasso CL, Borri M (1997) Energy preserving/decaying schemes for non-linear beam dynamics using the helicoidal approximation. Comput. Meth. Appl. Mech. Eng. 143: 393–415

Botasso CL, Borri M, Trainelli L (2001) Integration of elastic multibody systems by invariant conserving/dissipating algorithms. II. Numerical schemes and applications. Comput. Meth. Appl. Mech. Eng. 190: 3701–3733

Cardona A, Geradin M (1989) Time integration of the equations of motion in mechanism analysis. Comput. Struct. 33(3): 801–820

Cosserat E, Cosserat F (1909) Théorie des corps déformables, Traité de Physique. Paris, second edition

Crisfield MA (1997) Non-linear finite element analysis of solids and structures. vol. 2: Advanced Topics, John-Wiley & Sons, Chichester

Crisfield MA, Galvanetto U, Jelenić G (1997) Dynamics of 3D co-rotational beams. Comput. Mech. 20: 507–519

Crisfield MA, Jelenić G (1998) Objectivity of strain measures in geometrically exact 3D beam theory and its finite element implementation. Proc. Roy. Soc. London 455: 1125–1147

Crisfield M, Shi J (1994) A Co-rotational element/time-integration strategy for non-linear dynamics. Int. J. Numer. Meth. Eng. 37, 1897–1913

Galvanetto U, Crisfield MA (1996) An energy-conserving co-rotational procedure for the dynamics of planar beam structures. Int. J. Numer. Meth. Eng. 39: 2265–2282

González O (2000) Exact energy-momentum conserving algorithms for general models in nonlinear elasticity. Comput. Meth. Appl. Mech. Eng. 190: 1763–1783

Gruttman F, Sauer R, Wagner W (1998) A geometrically nonlinear eccentric 3D-beam element with arbitrary cross-sections. Comput. Meth. Appl. Mech. Eng. 160: 383–400

Hairer E, Wanner G (1991) Solving Ordinary Differential Equations II: Stiff and Differential-Algebraic Problems, Springer-Verlag, Berlin

Hilber HM, Hughes TJR, Taylor RL (1977) Improved numerical dissipation for time integration algorithms in structural dynamics. Earthquake Eng. Struct. Dynamics 5: 283–292

Hughes TJR (1987) The finite element method. Prentice-Hall

Ibrahimbegovic A (1995) On finite element implementation of geometrically nonlinear Reissner's beam theory: three-dimensional curved beam elements. Comput. Meth. Appl. Mech. Eng. 122: 11–26

Jelenić G, Crisfield MA (1998) Interpolation of rotational variables in nonlinear dynamics of 3D beams. Int. J. Numer. Meth. Eng. 43: 1193–1222

Jelenić G, Crisfield MA (1999) Geometrically exact 3d beam theory: implementation of a strain-invariant finite element for statics and dynamics. Comput. Meth. Appl. Mech. Eng. 171: 141–171

Jelenić G, Crisfield MA (2000) Dynamic analysis of 3D beams with joints in presence of large rotations. Comput. Meth. Appl. Mech. Eng. (in press)

Kane C, Marsden JE, Ortiz M, West M (2000) Variational integrators and the Newmark algorithm for conservative and dissipative mechanical systems. Int. J. Numer. Meth. Eng. 49, 1295–1325

Kuhl D, Crisfield MA (1997) Energy conserving and decaying algorithms in non-linear structural dynamics. Int. J. Numer. Meth. Eng. 45: 569–599

Kuhl D, Ramm E (1996) Constraint energy momentum algorithm and its application to non-linear dynamics of shells. Comput. Meth. App. Mech. Eng. 136: 293–315

Kuhl D, Ramm E (1999) Generalized energy–momentum method for nonlinear adaptive shell analysis. Comput. Meth. App. Mech. Eng. 178: 343–366

Prothero A, Robinson A (1974) On the stability and accuracy of one-step methods for solving stiff systems of ordinary differential equations. Math. Comput. 28: 145–162

Reissner E (1972) A one-dimensional finite strain beam theory: the plane problem. J. Appl. Math. Phys. (ZAMP) 23: 795–804

Romero I, Armero F (2002a) An objective finite element approximation of the kinematics of geometrically exact rods and its use in the formulation of an energy-momentum conserving scheme. Int. J. Numer. Meth. Eng. 54: 1683–1716

Romero I, Armero F (2002b) Numerical integration of the stiff dynamics of geometrically exact shells. Int. J. Numer. Meth. Eng. 54: 1043–1086

Simo JC (1985) A three-dimensional finite-strain rod model. Part I. The three-dimensional dynamic problem. Comput. Meth. Appl. Mech. Eng. 72(3): 267–304

Simo JC, Tarnow N (1992) The discrete energy–momentum method. conserving algorithms for nonlinear elastodynamics. ZAMP 43: 757–793

Simo JC, Tarnow N, Doblaré M (1995) Non-linear dynamics of three-dimensional rods: exact energy and momentum conserving algorithms. Int. J. Numer. Meth. Eng. 38(9): 1431–1473

Simo JC, Vu-Quoc L (1988) On the dynamics in space of rods undergoing large motions – a geometrically exact approach. Comput. Meth. Appl. Mech. Eng. 66(2): 125–161

Wilson EL (1968) A computer program for the dynamic stress analysis of underground structures. SEL Report 68-1, University of California at Berkeley